Gondwana Research 121 (2023) 168–195

Contents lists available at ScienceDirect

Gondwana Research

journal homepage: www.elsevier.com/locate/gr

The South Armenian Block: Gondwanan origin and Tethyan evolution in space and time

Igor K. Nikogosian [a,b,*], Antoine J.J. Bracco Gartner [a,b], Paul R.D. Mason [b], Douwe J.J. van Hinsbergen [b], Klaudia F. Kuiper [a], Uwe Kirscher [c,d], Sergei Matveev [b], Araik Grigoryan [e], Edmond Grigoryan [e], Arsen Israyelyan [e], Manfred J. van Bergen [b], Janne M. Koornneef [a], Jan R. Wijbrans [a], Gareth R. Davies [a], Khachatur Meliksetian [e]

[a] Faculty of Science, Vrije Universiteit Amsterdam, De Boelelaan 1085, 1081 HV Amsterdam, The Netherlands
[b] Department of Earth Sciences, Utrecht University, Princetonlaan 8a, 3584 CB Utrecht, The Netherlands
[c] Earth Dynamics Research Group, The Institute for Geoscience Research (TIGeR), School of Earth and Planetary Sciences, Curtin University, Bentley, Western Australia 6102, Australia
[d] Department of Geosciences, University of Tübingen, Schnarrenbergstraße 94–96, 72076 Tübingen, Germany
[e] Institute of Geological Sciences, Armenian National Academy of Sciences, 24a Marshal Baghramyan Ave, Yerevan 0019, Armenia

ARTICLE INFO

Article history:
Received 25 November 2022
Revised 2 March 2023
Accepted 31 March 2023
Available online 6 April 2023
Handling editor: A. Festa

Keywords:
South Armenian Block
Metamorphic basement
Igneous intrusions
Cimmerian continent
Geodynamic evolution

ABSTRACT

The geodynamic evolution of the South Armenian Block (SAB) within the Tethyan realm during the Palaeozoic to present-day is poorly constrained. Much of the SAB is covered by Cenozoic sediments so that the relationships between the SAB and the neighbouring terranes of Central Iran, the Pontides and Taurides are unclear. Here we present new geochronological, palaeomagnetic, and geochemical constraints to shed light on the Gondwanan and Cimmerian provenance of the SAB, timing of its rifting, and geodynamic evolution since the Permian. We report new $^{40}Ar/^{39}Ar$ and zircon U-Pb ages and compositional data on magmatic sills and dykes in the Late Devonian sedimentary cover, as well as metamorphic rocks that constitute part of the SAB basement. Zircon age distributions, ranging from ~3.6 Ga to 100 Ma, firmly establish a Gondwanan origin for the SAB. Trondhjemite intrusions into the basement at ~263 Ma are consistent with a SW-dipping active continental margin. Mafic intraplate intrusions at ~246 Ma (OIB) and ~234 Ma (P-MORB) in the sedimentary cover likely represent the incipient stages of breakup of the NE Gondwanan margin and opening of the Neotethys. Andesitic dykes at ~117 Ma testify to the melting of subduction-modified lithosphere. In contrast to current interpretations, we show that the SAB should be considered separate from the Taurides, and that the Armenian ophiolite complexes formed chiefly in the Eurasian forearc. Based on the new constraints, we provide a geodynamic reconstruction of the SAB since the Permian, in which it started rifting from Gondwana alongside the Pontides, likely reached the Iranian margin in Early Jurassic times, and was subject to episodes of intraplate (~189 Ma) and NE-dipping subduction-related (~117 Ma) magmatism.

1. Introduction

The present-day tectonic setting of the Arabian-Eurasian collision zone is the result of a complex Late Palaeozoic to Cenozoic geodynamic evolution that is partially preserved in large-scale tectono-stratigraphic terranes stretching from the Mediterranean to Tibet. Integral to this evolution is the Permian breakup of Gondwana and the formation of a collection of microcontinents in the Tethyan realm, termed Cimmeria (Şengör and Yilmaz, 1981), which drifted away from the NE margin of Gondwana during the Permian–Triassic as the Neotethys Ocean opened (e.g., Stampfli and Borel, 2002; Torsvik and Cocks, 2013). These terranes, presently stretching from Turkey to southern China, have successively amalgamated to the southern Eurasian continental margin during the Mesozoic and Cenozoic, closing the Palaeotethys and Neotethys Oceans.

One of these Gondwana-derived fragments is the South Armenian Block (SAB; Knipper and Khain, 1980), a continental fragment presently separated from the former southern Eurasian margin by the Sevan–Akera suture zone in the north and east, and juxtaposed

* Corresponding author at: Faculty of Science, Vrije Universiteit Amsterdam, De Boelelaan 1085, 1081 HV Amsterdam, The Netherlands.
E-mail address: i.k.nikogosian@vu.nl (I.K. Nikogosian).

https://doi.org/10.1016/j.gr.2023.03.023
1342-937X/

along another ophiolite-bearing suture zone against the easternmost Taurides and Iran to the south (Fig. 1; Knipper, 1975; Adamia et al., 1981). Its kinematic evolution within the Tethyan realm between the Permian and Late Cretaceous remains enigmatic, chiefly because of the limited amount of available geological evidence. Although its Gondwanan origin has long been inferred (Belov and Sokolov, 1973; Aghamalyan, 1978), its affinity with neighbouring Gondwana-derived terranes, especially Central Iran, the Pontides and the Taurides, is not well-understood. In the absence of palaeomagnetic constraints on the position of the SAB during its northward drift, it has been interpreted as a contiguous part of Iran (e.g., Stampfli et al., 1991; Brunet et al., 2003; Adamia et al., 2017), the Taurides (e.g., Okay and Tüysüz, 1999; Barrier and Vrielynck, 2008; Rolland et al., 2012; Meijers et al., 2015), and as a separate micro-continent (van Hinsbergen et al., 2020). Moreover, no unequivocal constraints have yet been placed on the timing of rifting of the SAB from the Gondwanan margin and, as a result, the inferred ages range from Late Permian (~260 Ma) to Early Jurassic (~174 Ma) (Şengör and Yilmaz, 1981; Mart, 1987; Gealey, 1988; Kazmin, 1991; Bazhenov et al., 1996; Stampfli and Borel, 2002; Robertson et al., 2004; Moix et al., 2008).

Currently no consensus exists on the provenance and geodynamic evolution of the SAB within the Tethyan realm. Key questions yet to be answered by observational data include: (1) When did the SAB start drifting from the Gondwanan margin?; (2) What is its relation to the neighbouring terranes of present-day Turkey and Iran?; and (3) How did the SAB evolve and interact in the Mesozoic Tethyan realm? Here, we present the first U-Pb geochronological and trace-element data on zircons, coupled with geochemical compositions of their metamorphic host rocks that

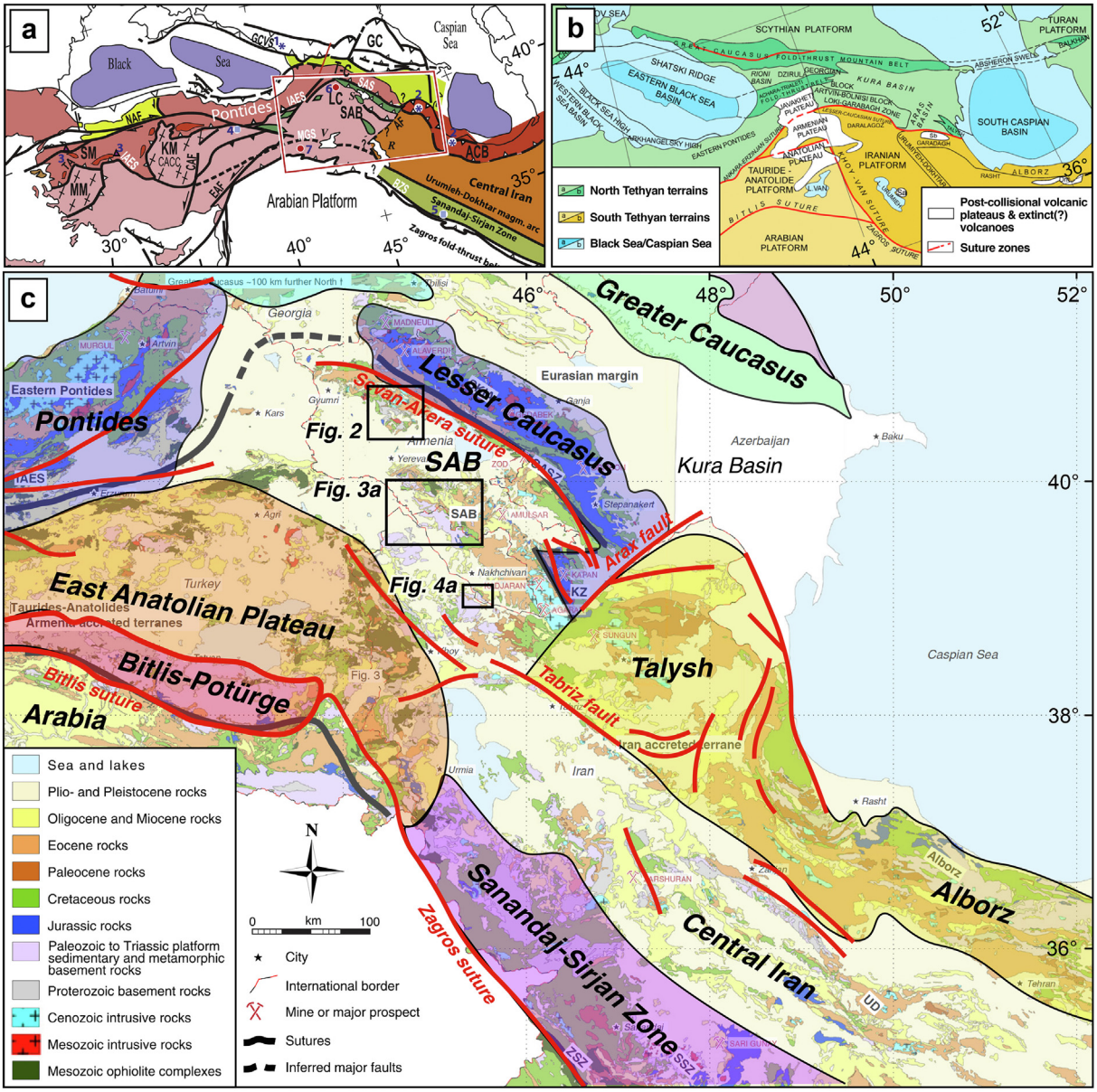

Fig. 1. Tectonic maps of the circum-Caucasian region. (a-b) Maps presented in recent review papers by Rolland (2017) and Adamia et al. (2017), respectively, illustrating the ambiguous tectonic affinity of the South Armenian Block. (c) Geological map of the Tethyan belt from eastern Turkey to western Iran, highlighting the Lesser Caucasus, Mesozoic and Cenozoic intrusive rocks and ophiolites (after Mederer et al., 2014, and references therein) and main tectonic units (van der Boon et al., 2018, and references therein). IAES = Izmir-Ankara-Erzincan suture; SAB = South Armenian Block; SASZ = Sevan Akera suture zone; SKIA = Somkheto Karabakh Island Arc; SSZ = Sanandaj-Sirjan zone; UD = Urumieh Dokhtar magmatic arc; ZSZ = Zagros suture zone.

constitute part of the uplifted SAB basement, as well as $^{40}Ar/^{39}Ar$ ages and Sr-Nd-Pb isotope and geochemical compositions of hitherto unreported mafic to intermediate Mesozoic magmatism in the Late Devonian sedimentary cover of the SAB. These new results are used to reconstruct the geodynamic history of the SAB and interpret its evolution in the context of the Permian–Triassic breakup of the NE Gondwanan margin and the Mesozoic kinematic history of the Tethyan realm.

2. Geological setting

The Middle East–Caucasus region comprises a series of Gondwana-derived continental blocks that successively accreted to the southern Eurasian margin upon closure of the Palaeotethys and Neotethys Oceans in Palaeozoic to Cenozoic times (e.g., Barrier and Vrielynck, 2008). Here the focus is on the SAB, the central region between the contrasting palaeotectonic settings of Turkey and Iran (Fig. 1).

2.1. Iran

In Iran, Gondwana-derived Cimmerian blocks amalgamated to the Eurasian margin during the Late Triassic (Mouthereau et al., 2012; McQuarrie and van Hinsbergen, 2013) as a result of the northward subduction and closure of the Palaeotethys ocean during Permian–Triassic times (Berberian and King, 1981; Şengör, 1987; Stampfli, 2000). The Central Iranian block later separated into multiple continental domains due to the opening of back-arc basins (from E to W: Lut, Tabas, Yazd; Fig. 1), and are now separated by sutures with remnants of Cretaceous ophiolites (Shafaii Moghadam and Stern, 2015) and major faults (Alavi, 1991). These domains, often termed "Cadomian", contain Ediacaran–Cambrian (600–520 Ma) crust (Hassanzadeh et al., 2008; Azizi et al., 2011; Jamshidi Badr et al., 2013; Shafaii Moghadam et al., 2015). This Central Iranian block is bounded to the north by sutures in the Alborz and Kopet-Dagh mountains, to the east by the Sistan suture zone, and to the south by the Neotethys suture and the Arabia-derived Zagros fold-and-thrust belt (see Agard et al., 2011; Shafaii Moghadam and Stern, 2014). The Sanandaj-Sirjan zone, extending from NW to SE Iran, hosts a volcanic arc of Jurassic and younger age (e.g., Berberian and King, 1981; Şengör, 1990; Sheikholeslami et al., 2008; Fazlnia et al., 2009), widely interpreted to reflect northeastward subduction of the Neotethys since the Jurassic (Berberian and King, 1981; Davoudzadeh and Schmidt, 1981) or Late Jurassic times (Mohajjel and Fergusson, 2000). Regardless of the interpretation of the Sanandaj-Sirjan Zone, Neotethys Ocean subducted beneath the Iranian Cimmerian blocks from Jurassic times until Arabia collided with Eurasia (Agard et al., 2011).

2.2. Turkey

Turkey's tectonic history is markedly different from that of Iran. Two continent-derived fold-and-thrust belts—the Pontides and the Anatolide-Tauride block—are separated by the Izmir-Ankara suture zone (Fig. 1). The Pontides has been part of the southern Eurasian margin since at least Jurassic time (Dokuz et al., 2017), and is thought to have drifted away from Gondwana during the Late Triassic (~240 Ma) reaching the southern Eurasian margin during the Early Jurassic, and opening the Neotethyan Ocean in its wake (~180 Ma; Şengör and Yilmaz, 1981; van Hinsbergen et al., 2020). Continental lithosphere of the Anatolide-Tauride block, in central and southern Turkey, separated from Gondwana during the Early Jurassic (200–190 Ma; van Hinsbergen et al., 2020). The Anatolides comprise several metamorphosed and exhumed massifs, such as the Kırşehir block, Tavşanlı zone, Afyon zone, and the Menderes massif. In contrast, the Taurides are composed of mainly non-metamorphosed sedimentary rocks in the form of a thin-skinned fold and thrust belt. Both Anatolide and Tauride units are buried below Late Cretaceous ophiolites (Özgül, 1984), where the Taurides host the non-metamorphosed, foreland accreted equivalents of some of the Anatolide massifs that were buried deeper (van Hinsbergen et al., 2016). The Pontides were once separated from the Anatolide-Tauride block by one or more strands of the Neotethys Ocean, relics of which are found in the form of mélanges and in ophiolites throughout Turkey (e.g., Yilmaz and Yilmaz, 2013; Dilek and Furnes, 2019). Much of eastern Anatolia is known as the Eastern Turkish High Plateau, which has long been described as a subduction-accretion prism (Şengör and Yilmaz, 1981; Şengör et al., 2019a). However, below the widespread Upper Neogene volcanic rocks of that plateau are Paleozoic to Cretaceous metamorphosed and non-metamorphosed continental rocks that are overlain by Cretaceous ophiolites and intruded by Upper Cretaceous and younger volcanic arc rocks (Kuscu et al., 2010; Yilmaz et al., 2010; Topuz et al., 2017). These rocks are equivalent to the northern Taurides and show that continental crust of the Taurides continues to the Iran-Turkey border (van Hinsbergen et al., 2020).

2.3. South Armenian Block

The Lesser Caucasus and Armenian Highland form a central region between the contrasting palaeotectonic systems of Turkey and Iran. These regions were separated by a plate boundary since Permian times (Stampfli and Borel, 2002), likely in the form of a major transform fault system. Palaeogeographic reconstructions suggest that this fault system could have been reactivated since the Early Eocene (Barrier and Vrielynck, 2008). The Arax valley fault (Fig. 1c; Jackson and McKenzie, 1984) has been suggested to be a vestige of this transform system, based on substantial differences in convergence between the Lesser Caucasus and Talysh of NW Iran (van der Boon et al., 2018).

The Lesser Caucasus, located south-west of the Greater Caucasus (Fig. 1c), represents a Jurassic-to-Eocene volcanic arc (Somkheto-Karabakh arc) built along the Eurasian continental margin and is considered part of the regional Pontide–Lesser Caucasus–Alborz volcanic palaeo-arc system (Lordkipanidze, 1980). Its southern and south-western border with the SAB is marked by the Sevan-Akera suture (Knipper, 1975; Adamia et al., 1980) that is demarcated by a belt of Jurassic ophiolites (Amasia, Sevan, and Stepanavan) that forms part of a regional ophiolite suture zone extending further west to the Ankara–Erzincan ophiolites south of the Pontides (Knipper and Khain, 1980; Hässig et al., 2013b). These ophiolites contain ~170–180 Ma oceanic crust, suggested to have formed in the upper plate of a Jurassic subduction zone (Galoyan et al., 2007, 2009; Rolland et al., 2010; Hässig et al., 2013a; Topuz et al., 2013a, 2013b). They are overlain by pillow lavas or Middle–Upper Jurassic radiolarian cherts (Danelian et al., 2006, 2010, 2016). The Sevan-Akera suture zone also hosts an ophiolite-derived, Coniacian–Santonian (~84–90 Ma) flysch (Sosson et al., 2010, and references therein), which unconformably overlies the ophiolites as a forearc basin deposit, and which connects to the Lesser Caucasus arc. This demonstrates that the Jurassic ophiolites formed the Lesser Caucasus forearc and that ophiolite obduction effectively dates the collision of the SAB and Lesser Caucasus (van Hinsbergen et al., 2020), as is the case in the eastern Pontides (Topuz et al., 2014).

The continental SAB is generally assumed to be of *peri*-Gondwanan origin, owing to its Proterozoic metamorphic basement ages (Knipper and Khain, 1980; Aghamalyan, 2004). This metamorphic basement is of Cadomian–Neoproterozoic age and outcrops in the Tsakhkunyats Massif, 40 km north of Yerevan

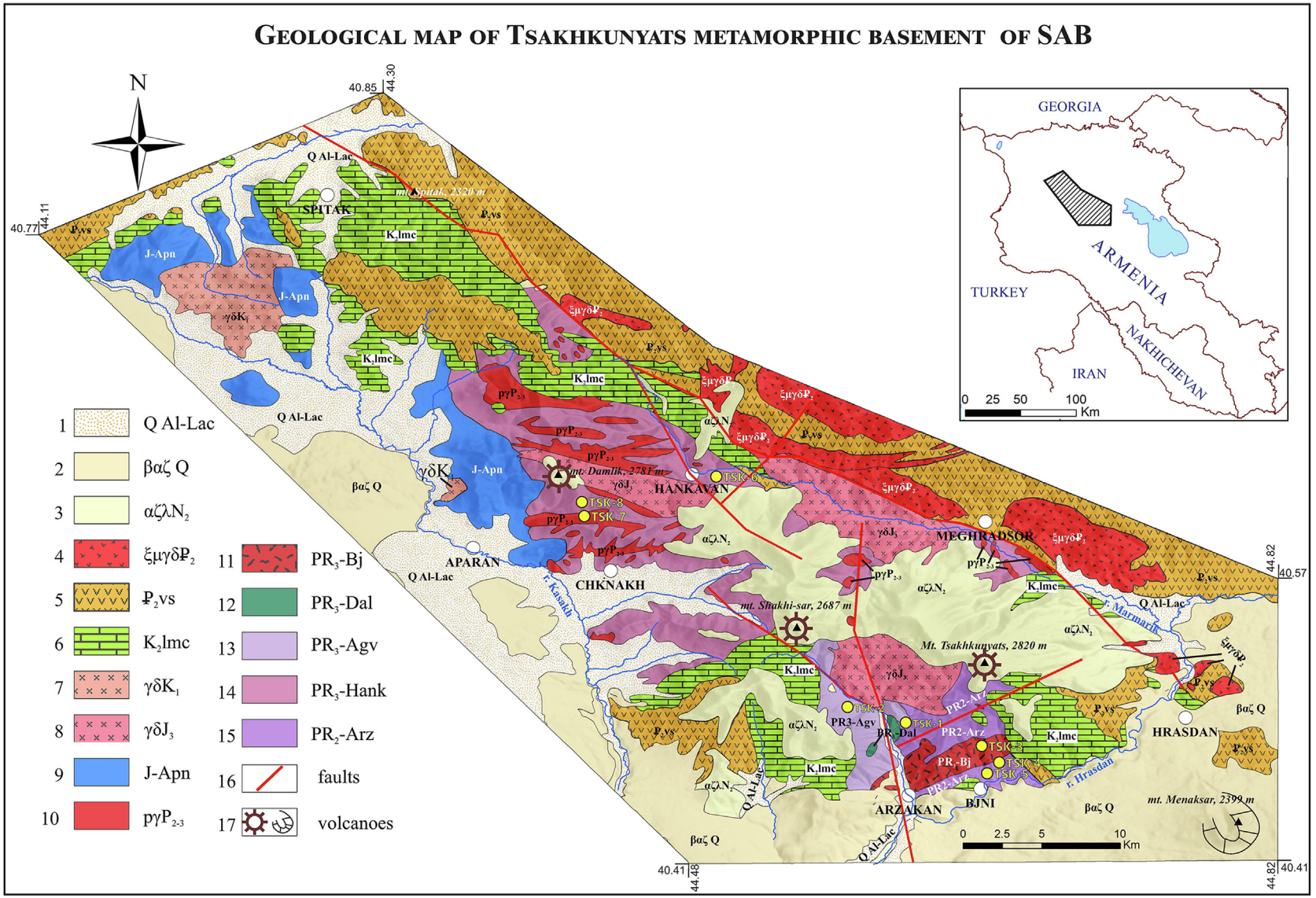

Fig. 2. Geological map of the Tsakhkunyats metamorphic basement of the SAB compiled with use of maps and sections by Paffenholz (1952), Arakelyan (1957), Aghamalyan (1983), Meliksetian (1989), Kharazyan (2005), and the authors' data. Locations of the studied samples with prefix "TSK-" are shown. Legend: *Pliocene-Quaternary*. 1. Q Al-Lac = Quaternary alluvial and lacustrine clastic de- posits; 2. βαζ Q = Quaternary volcanic series: lava flows of basaltic andesites, andesites, dacites and pyroclastic deposits; 3. $\alpha\zeta\lambda N_2$ = Pliocene volcanic series: lava flows of andesites, dacites, rhyolites, and pyroclastic deposits. *Eocene*. 4. $\xi\mu\gamma\delta P_2$ = Middle Eocene Tezhsar, Aghavnadsor and Meghradsor intrusive complexes: alkali pseudoleucite and nepheline syenites, monzonites, syenogranites, diorites, monzodiorites (39.5–42.4 Ma; ages after Sokół et al., 2018; Grosjean et al., 2022); 5. P_2vs = Middle Eocene volcanic, volcano-sedimentary and sedimentary suite. *Upper Cretaceous*. 6. K_2lmc = Upper Cretaceous: limestones, marls, conglomerates; 7. $\gamma\delta K_1$ =Lower Cretaceous tonalitic intrusive formation, Gegharot and Mirak intrusives, tonalites and granodiorites (140–143 Ma; Galoyan et al., 2020). *Jurassic*. 8. $\gamma\delta J_3$ = Upper Jurassic tonalitic intrusive formation, Aghveran, Artavaz and Hankavan intrusives, tonalites and granodiorites (155–161 Ma; Galoyan et al., 2020); 9. J-Apn = Jurassic (?) Aparan volcanic, volcano-sedimentary suite and sedimentary suite. *Late Palaeozoic*. 10. $p\gamma P_{2-3}$ = Middle–Late Permian trondhjemite (plagiogranite) intrusive complex (262.5 ± 4.3 Ma; this work and 250–270 Ma after Galoyan et al., 2020). *Precambrian*. 11. PR_3-Bj = Neoproterozoic: Bjni metamorphic complex, granite-gneisses and migmatites (558 ± 14 Ma; this work and 533–554 Ma after Galoyan et al., 2020); 12. PR_3-Dal = Neoproterozoic: Dalar metagabbro-amphibolites; 13. PR_3-Agv = Neoproterozoic: Aghveran suite, phyllites, metavolcanic, green schists, mica schists metamorphic suite; 14. PR_3-Hank = Neoproterozoic Hankavan metamorphic complex, amphibolites, epidote-amphibole green schists, mica schists and marbles; 15. PR_2-Arz = Mesoproterozoic: Arzakan suite, quartz-mica schists, graphite- almandine-andalusite-mica schists, marbles. 16 = Faults; 17 = Pliocene and Quaternary volcanic centres. (For interpretation of the references to colour in this figure legend, the reader is referred to the web version of this article.)

(Fig. 1c) (Belov and Sokolov, 1973; Aghamalyan, 1998). It comprises the Precambrian Arzakan and Hankavan complexes (Fig. 2), which contain various mica schists, gneisses as well as amphibolites, metamorphic basic and ultrabasic rocks, considered to represent slices of the Pan-African oceanic crust (Aghamalyan et al., 2011). The SAB is covered by a platform sedimentary sequence consisting of folded Upper Devonian to Upper Triassic sedimentary formations (Aslanyan, 1958; Arakelyan, 1964).

In recent years, the SAB is often assumed to be part of the Anatolide-Tauride block, based on similarities in basement, stratigraphy and especially the obduction ages for the Jurassic Sevan-Akera ophiolites in the Late Cretaceous (e.g., Barrier and Vrielynck, 2008; Rolland et al., 2012; Hässig et al., 2013a; Meijers et al., 2015; Menant et al., 2016; Hässig et al., 2017). In a Mesozoic–Cenozoic kinematic reconstruction of the Mediterranean, van Hinsbergen et al. (2020) provide a comprehensive interpretation of the SAB's tectonic contacts with neighbouring blocks and proposed an alternative model. They infer that a suture zone (Yilmaz et al., 2014), termed Kağızman-Khoy suture, separates the SAB from the easternmost Taurides. It consists of a belt of ophiolites extending from the Kağızman ophiolite (easternmost Turkey) to the Khoy ophiolite (NW Iran near the Turkish border). Two different subduction systems were involved: the first was intra-oceanic and emplaced Cretaceous supra-subduction zone ophiolites onto the Taurides (causing ~78–83 Ma metamorphism; Topuz et al., 2017), whereas the second closed the ocean basin and juxtaposed the easternmost Taurides and the SAB. Van Hinsbergen et al. (2020) note that the latter closure likely happened after ~75–80 Ma, when the SAB collided with the Transcaucasus (Rolland et al., 2012) and as a consequence the subduction system moved south.

Van Hinsbergen et al. (2020) further interpreted that the SAB detached from the Gondwanan continent at ~240 Ma as part of the Pontides, and separated it from the Pontides by a ridge jump at ~230 Ma. In contrast, uncoupling of the Taurides from Gondwana did not start earlier than ~190–200 Ma (van Hinsbergen et al., 2020).

3. Samples

3.1. Metamorphic basement

The sampled Pan-African (Cadomian–Neoproterozoic) basement that outcrops in the Tsakhkunyats Massif, 40 km north of Yerevan, includes two Precambrian complexes: (1) Arzakan and (2) Hankavan (Fig. 2; Aghamalyan, 2004). The Arzakan complex (from which samples TSK-1 to 5 were taken; Table 1) consists of 1500-m thick paraschists metamorphosed in the almandine-amphibolite facies, and 2000-m thick metavolcanics, phyllites (sample TSK-5), marbles, and schists metamorphosed in the greenschist facies (Adamia et al., 2011). The complex is intruded by granite-gneisses (sample TSK-3) having a Rb/Sr isochron age of 620 Ma (Aghamalyan, 2004) and zircon U-Pb ages of 533–554 Ma (Galoyan et al., 2020). The 1900-m thick lower part of the Hankavan complex was obducted over the Arzakan complex during the Pan-African orogenic events. It represents an oceanic crust–type assemblage, predominantly containing metakomatiite-basalt amphibolites (sample TSK-8) with thin sedimentary intercalations (Adamia et al., 2011). The 1000-m thick upper part of the Hankavan complex consists of metabasalt and metaandesite with beds of marble and quartz-mica schists (sample TSK-6). Both parts of the complex contain serpentinite lenses. The complex is cut by trondhjemite (plagiogranite) intrusions (sample TSK-7) having a Rb/Sr isochron age of 685 ± 77 Ma (Aghamalyan, 2004), while more recent U-Pb zircon dating yielded 250–270 Ma (Galoyan et al., 2020). Trondhjemite TSK-7 was also studied to obtain palaeomagnetic data (details in Supplementary Data S1). The petrography of the Tsakhkunyats rock samples are in Supplementary Data S2.

3.2. Mafic to intermediate sills and dykes

Fig. 3 shows the sedimentary cover of the SAB, which consists of folded Late Devonian to Late Triassic platform sediments (Aslanyan, 1958; Arakelyan, 1964). Mafic to intermediate sills and dykes penetrated this cover at several locations in Armenia and Nakhichevan, i.e., at Khor Virap (Ginter et al., 2011; Avagyan et al., 2018), Arpi (Arakelyan, 1952) and the Erakh-Negram zone in Nakhichevan (Khanzatian, 1992) (Fig. 4). For this study, Khor Virap and Arpi were sampled and analysed for the first time and results are integrated with geochemical and geochronological data reported for Negram and Darasham (Fig. 4; Karyakin, 1989; Khanzatian, 1992). The petrography of these rocks is in Supplementary Data S2.

The Khor Virap section, located 30 km south of Yerevan (Fig. 3b), consists of Upper Devonian–Lower Carboniferous shallow marine carbonates and siliciclastics (Ginter et al., 2011) with several distinct meter-scale mafic sills exposed on the hills near the Khor Virap monastery (Fig. 3). The section forms part of the Ararat depression, which is filled mostly by Quaternary lacustrine sediments, and represents an uplifted unit situated on a horst (Milanovsky, 1968) or related to local contractional tectonics associated with thrust faulting (Avagyan et al., 2015). The three sills (samples KV-1, KV-2, KV-3) lie conformably within the Famennian sedimentary units (Fig. 3b; Ginter et al., 2011). KV-3 is sampled from the largest well-exposed sill (~4 m thick), located between limestone (upper contact) and siliciclastics (lower contact) with well-pronounced thermal contacts on both sides (Fig. 3d). The KV-1 sill as well as an adjacent quartzite (metamorphosed Upper Devonian sandstone) were studied to obtain palaeomagnetic data (details in Supplementary Data S1).

The Arpi area (Ertych section; Serobyan et al., 2019), located 60 km SE of Khor Virap, also hosts several igneous sills and dykes. The sills (samples ARP-1, ARP-2 and ARP-4) also lie conformably within Famennian limestones and siliciclastics (Fig. 3c). In addition, well-exposed igneous dykes (samples ARP-3 and ARP-5) represent cross-cutting magmatic bodies interpreted as volcanic necks (Fig. 3f). In an earlier stratigraphic study on Upper Palaeozoic sediments (Arakelyan, 1952) these dykes were interpreted as centres of volcanic eruptions, although they were assumed to be of pre-Permian age. Sills ARP-1,4 and dyke ARP-3 were used to obtain palaeomagnetic data (details in Supplementary Data S1).

4. Methods

4.1. Whole-rock elements and isotopes

Whole-rock compositions of the studied samples were obtained by X-ray fluorescence spectrometry (XRF; for major elements) and inductively coupled plasma mass spectrometry (ICP-MS; for trace elements) at the Vrije Universiteit Amsterdam, using a Philips PW1404/10 XRF and Thermo Electron X-series-II ICP-MS, following the procedure of Klaver et al. (2017) and a modified procedure after Eggins et al. (1997), respectively. USGS reference material BHVO-2 was used as a secondary standard throughout ICP-MS analysis and indicated accuracy within 10% of the GeoReM preferred values (Jochum et al., 2016) for all reported trace elements (Supplementary Data S3). Uncertainties are typically < 2% (2 RSD) for major oxides and < 5% (2 RSD) for trace elements.

Table 1
Metamorphic basement and igneous intrusive rock sample information. Tectonic units refer to the legend shown in Fig. 2. [1] Ginter et al. (2011).

Location/sample	Latitude	Longitude	Tectonic unit	Lithology	Location description
Metamorphic basement rocks					
Arzakan complex					
TSK-1	40.485868	44.5965475	PR_2-Arz (Bjni suite)	Mica schist	4.1 km N of Arzakan
TSK-2	40.503482	44.580787	PR_3-Agv (Aghveran suite)	Metarhyolite	6.4 km NNW of Arzakan
TSK-3	40.471182	44.647065	PR_3-Bj (Granito-gneiss Fm; Bjni massif)	Granite-gneiss	2.0 km N of Bjni (Vankidzore valley)
TSK-4	40.467222	44.648081	PR_2-Arz (Vankidzore suite)	Mica schist	1.5 km N of Bjni (Vankidzore valley)
TSK-5	40.464362	44.647855	PR_2-Arz - $PR_{3-?}$ (Berditak suite)	Metaarkose phyllite	1.2 km N of Bjni (Vankidzore valley)
Hankavan complex					
TSK-6	40.639147	44.506208	PR_3-Hank (Hankavan suite)	Green schist (metapelite)	1.8 km ENE of Hankavan (Marmarik valley)
TSK-7	40.61916	44.421675	$p\gamma P_{2-3}$ (Middle-Late Permian trondhjemite intrusive complex)	Trondhjemite	3.5 km ENE of Lusagyugh
TSK-8	40.61916	44.421675	PR_3 (Hankavan complex, Kasakh)	Metakomatiite basalt amphibolite	3.5 km ENE of Lusagyugh
Igneous intrusive rocks			**Country rock and age**		
Khor Virap					
KV-1	39.881272	44.573578	Famennian carbonates-siliciclastics [1]	Basalt	500 m NNW of Khor Virap monastery
KV-2	39.883244	44.574600	"	Basalt	"
KV-3	39.883739	44.575414	"	Basalt	"
Arpi					
ARP-1	39.733733	45.248772	Famennian limestones	Basalt	1 km SW of Arpi village
ARP-2	39.733775	45.249217	"	Basalt	"
ARP-3	39.730550	45.252692	"	Andesite	"
ARP-4	39.731139	45.253100	"	Basalt	"
ARP-5	39.732011	45.253333	"	Andesite	"

Isotope analyses for U, Pb and Sm, as well as Nd in samples ARP-3 and ARP-4, were conducted using a Thermo Fisher Neptune Multicollector (MC-)ICP-MS, following standard procedures (Font et al., 2012). Neodymium (for samples KV-1,2 and ARP-1, due to low Nd contents) and Sr isotope compositions were measured by thermal ionisation mass spectrometry (TIMS) using a Thermo Scientific Triton Plus instrument, following procedures outlined in Koornneef et al. (2013) and Klaver et al. (2015). Rubidium was measured by TIMS on a Finnigan MAT 262 RPQ-plus running in static mode. Small, 20–30 ng aliquots of synthetic reference materials (JNdi-1, NBS-987 Sr and NBS-984 Rb) were measured alongside the respective samples to check for accuracy and reproducibility ($^{143}Nd/^{144}Nd$ = 0.512101 ± 0.000011 2SD, n = 2; $^{87}Sr/^{86}Sr$ = 0.710254 ± 0.000021, n = 3; $(^{85}Rb/^{87}Rb)_{raw}$ = 2.627 ± 0.006, n = 4; respectively). Total procedural blanks (from sample dissolution to loading on filament) were 22 pg for Sr, 100 pg for Rb, 0.04 pg for Nd and 42 pg for Pb, and are insignificant in comparison to the amounts of respective elements analysed. USGS reference material BHVO-2 was included throughout to validate the chromatographic and analytical procedures.

Age corrections were applied to the isotopic values to allow evaluation of initial ratios (denoted with the subscript i). Parental/-daughter ratios were calculated using atomic and isotopic constants by De Laeter et al., (2003) and age corrections were performed using conventional decay constants. Initial ε_{Nd} values $[(\varepsilon_{Nd})_i]$ were calculated assuming $(^{143}Nd/^{144}Nd)^{o}_{CHUR}$ = 0.512638 (Bouvier et al., 2008) and $(^{147}Sm/^{144}Nd)^{o}_{CHUR}$ = 0.1967 (Jacobsen and Wasserburg, 1980).

4.2. Zircon trace elements and U-Pb isotopes

Zircon grains were separated from the crushed fractions of samples TSK-1,3,5,7 and ARP-1,3,5 by conventional gravimetric (heavy liquid) and magnetic separation techniques at the Vrije Universiteit Amsterdam. They were handpicked under a binocular microscope, mounted in epoxy resin and polished to expose grain centres for characterisation of internal structures by back-scattered electron (BSE) and cathodoluminescence (CL) imaging at Utrecht University.

Zircon trace element and U-Pb isotope analyses were obtained by laser ablation (LA) ICP-MS, using a GeoLas 200Q Excimer laser ablation system (193-nm wavelength) coupled to a Thermo Finnigan Element 2 sector field ICP-MS instrument, at Utrecht University. The laser was operated using a spot size of 20–40 μm, a pulse repetition rate of 10 Hz and an energy density of 5 J/cm^2. For the trace-element analyses, offline time-integrated normalisation for instrumental drift was performed using the GLITTER software. For the trace-element analyses of zircons, the samples were calibrated to the NIST SRM 612 glass standard using an assumed fixed concentration of 32.45 wt% SiO_2 (151,684 ppm Si) in zircon (Anczkiewicz et al., 2001) measured on the interference-free isotope ^{29}Si. For U-Pb dating, the four Pb isotopes, ^{232}Th, ^{235}U and ^{238}U were measured. The 91500 zircon reference material (1,065 Ma; Wiedenbeck et al., 2004) was used as an external standard. Results for 91500 zircon ages yielded mean age of 1,065 ± 7 Ma (95% confidence level, MSDW = 0.72, probability = 0.92; Supplementary Fig. S1). Uncertainties for trace elements in zircon are typically smaller than 10% (2 RSD; Mason et al., 2008). U-Pb concordia diagrams, probability density plots and weighted averages were calculated using Isoplot 4. Cathodoluminescence images of the zircons with spot locations are in Supplementary Data S4.

4.3. $^{40}Ar/^{39}Ar$ dating

Samples KV-1, KV-2, ARP-3, and ARP-4 were crushed with a rock splitter and jaw crusher and consecutively washed and thoroughly cleaned in an ultrasonic bath. The samples were sieved into different size fractions. Phenocrysts were separated from the groundmass for sample ARP-4 and ~100 mg groundmass was irradiated together with a Drachenfels sanidine fluence monitor (25.

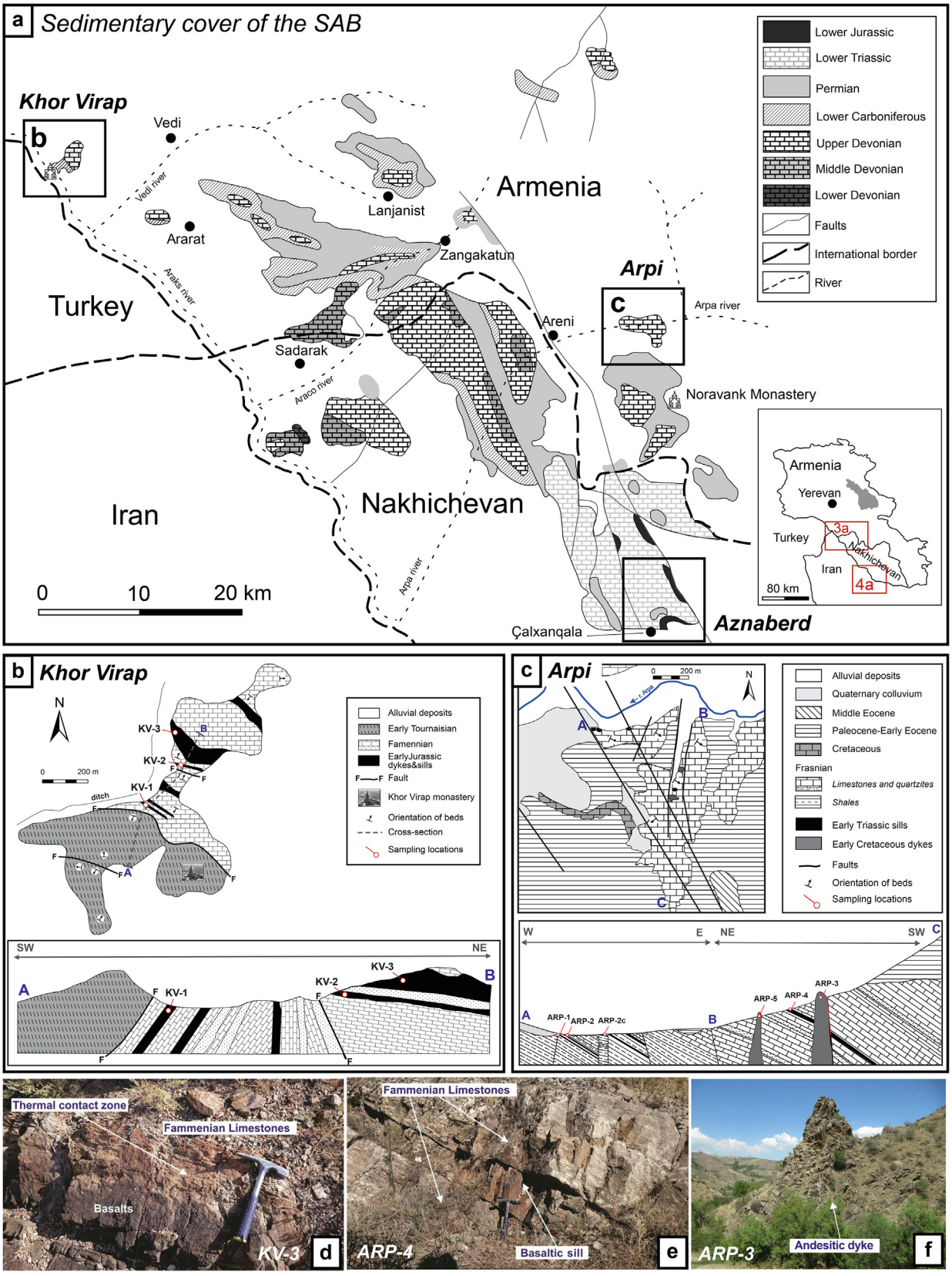

Fig. 3. (a) Schematic map of the south Armenian-Nakhichevan area, showing the distribution of Upper Devonian–Lower Carboniferous sediments and the locations of the Khor Virap and Arpi (Ertych) areas (modified after Serobyan et al., 2019). Geological maps and schematic cross-sections through the Middle Palaeozoic of (b) Khor Virap (redrawn and modified after Ginter et al., 2011) and (c) Arpi (this study) with sample localities (prefixes "KV-" and "ARP-", respectively). Field photographs of (d) Khor Virap sill KV-3, (e) Arpi sill ARP-4, and (f) Arpi dyke ARP-3 within the Frasnian–Famennian sediments.

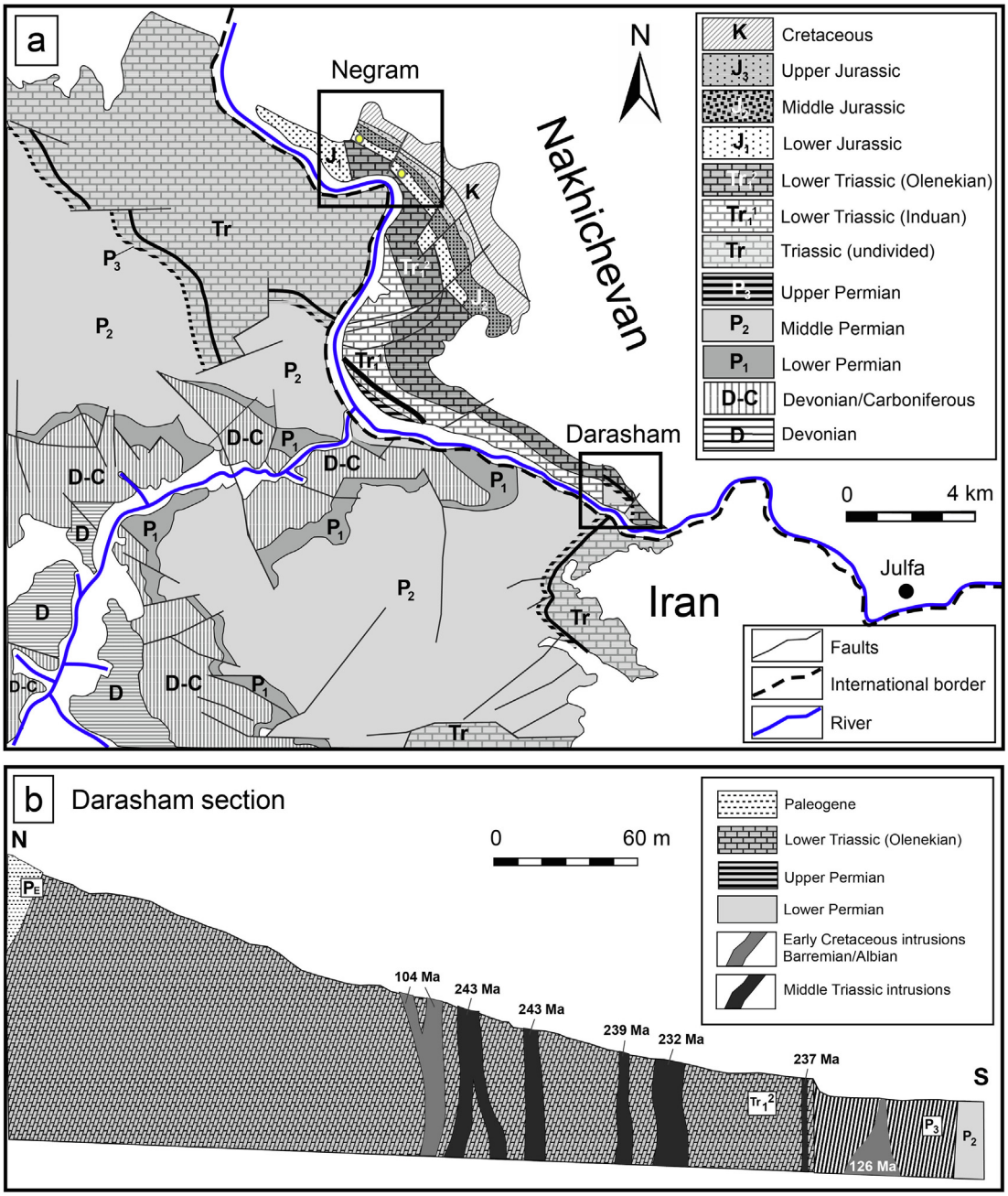

Fig. 4. (a) Simplified geological map of the south Nakhichevan area and adjacent part of NW Iran (modified after Alizadeh, 2008; Ghaderi et al., 2016), showing the distribution of Devonian to Cretaceous sediments and the locations of Lower Jurassic igneous rocks in the Negram area (studied by Karyakin, 1989; Bazhenov et al., 1996) and the Middle Triassic (232–243 Ma) and Early Cretaceous (104 and 126 Ma) igneous intrusions of the Darasham section (Khanzatian, 1992). (b) Cross-section of the Darasham section (redrawn after Khanzatian, 1992).

52 ± 0.08 Ma based on Wijbrans et al. (1995) and calibrated to Kuiper et al. (2008)) for 18 h in the Oregon State University Triga reactor, CLICIT facility (VU109). In addition, two plagioclase samples (KV-2, ARP-3) and one amphibole sample (KV-1) were separated using standard heavy liquid and magnetic mineral separation procedures and ~100 mg of each sample was irradiated in the same irradiation. All samples underwent a final hand-picking step under an optical microscope before irradiation.

$^{40}Ar/^{39}Ar$ analyses were performed at the geochronology laboratory of the Vrije Universiteit Amsterdam on a Helix MC noble gas mass spectrometer. Samples and standards were fused and/or incrementally heated with a Synrad CO_2 laser beam and released gas was exposed to a hot NP10 getter, a hot St172 getter, Ti sponge at 500 °C, a Lauda cooler at −70 °C and analysed on the Helix MC. The five argon isotopes were measured simultaneously with ^{40}Ar on the H2-Faraday position with a 10^{13} Ω resistor amplifier, ^{39}Ar on the H1-Faraday with a 10^{13} Ω resistor amplifier, ^{38}Ar on the AX-CDD, ^{37}Ar on the L1-CDD and ^{36}Ar on the L2-CDD (CDD = Compact Discrete Dynode). Gain calibration for the CDDs and Faraday cups is done by peak jumping a CO_2 reference beam on all detectors in dynamic mode. In a few cases calibration of Faraday cups was checked by peak jumping the ^{40}Ar beam between H2 and H1. All intensities were corrected relative to the L2 detector. Air pipettes were run every ten hours and were used for mass discrimination corrections. The atmospheric air value $^{40}Ar/^{36}Ar$ = 298.56 from Lee et al. (2006) was used in age calculations. Detailed analytical procedures for the Helix MC are described in Monster (2016). The correction factors for neutron interference

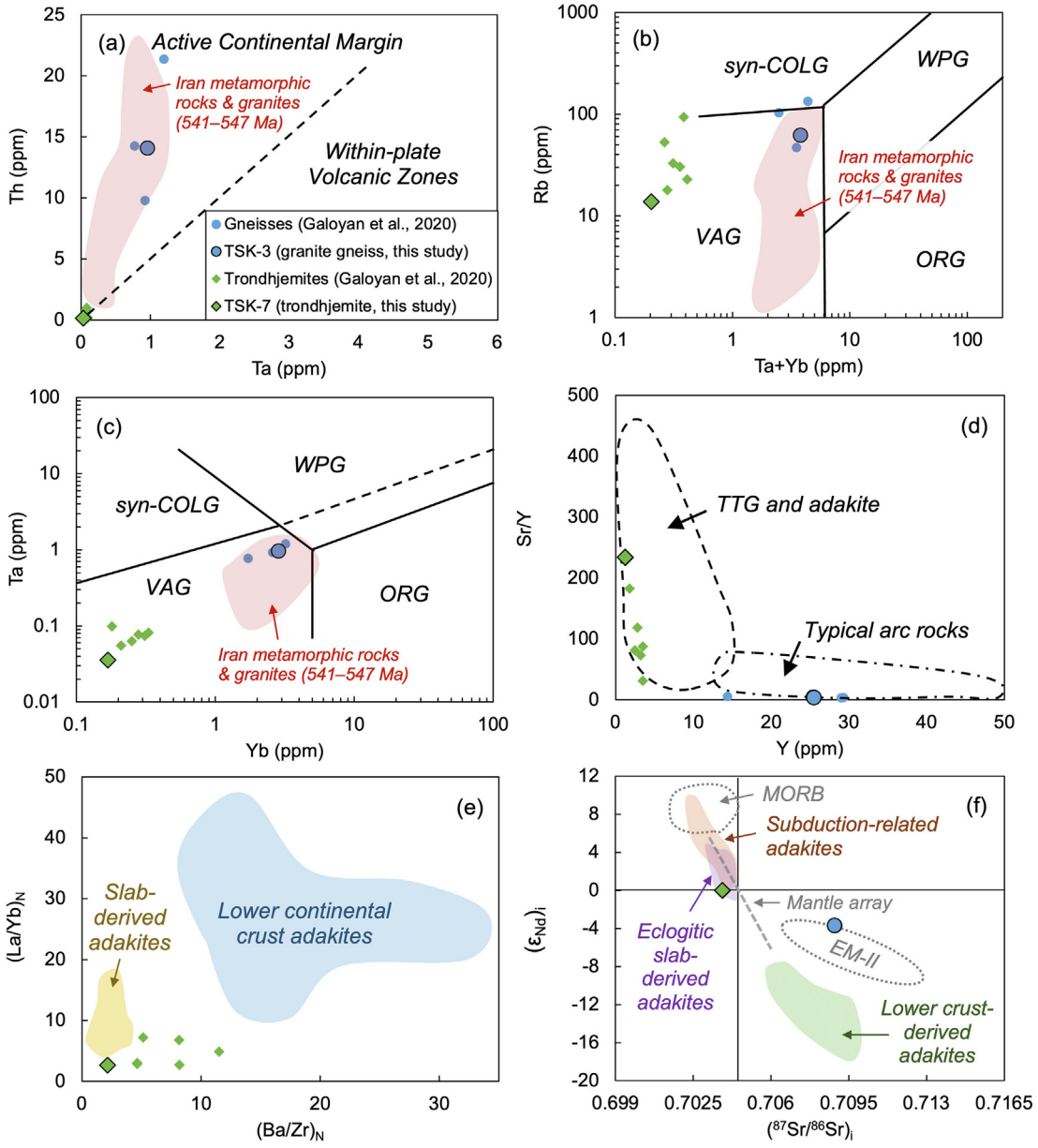

Fig. 5. Trace-element and Sr-Nd isotope diagrams for granite gneiss TSK-3 and trondhjemite TSK-7. (a) Th versus Ta (Schandl and Gorton, 2002). (b) Ta + Yb versus Rb (ppm) and (c) Yb versus Ta (ppm) (Pearce et al., 1984), illustrating the similarity between granite gneiss TSK-3 and granitic rocks associated with active continental margins and volcanic arcs and Neoproterozoic–Early Cambrian (541–547 Ma) subduction-related granitoids and metamorphic rocks from Iran (Balaghi Einalou et al., 2014). VAG = volcanic arc granites; ORG = ocean ridge granites; WPG = within-plate granites; COLG = collision granites. (d) Sr (ppm) versus Sr/Y (Defant and Drummond, 1990), with fields for typical arc rocks and TTG/adakites. (e) $(Ba/Zr)_N$ versus $(La/Yb)_N$, with fields for slab-derived adakites (Yogodzinski et al., 2015) and lower continental crust adakites (Hou et al., 2004). (f) $(^{87}Sr/^{86}Sr)_i$ versus $(\varepsilon_{Nd})_i$, with fields for MORB, EM-II (Willbold and Stracke, 2006), subduction-related adakites (Fan et al., 2022), eclogitic slab-derived adakites (Osozawa et al., 2019) and lower crust-derived adakites (Guan et al., 2012). Comparable data from rocks from the same respective metamorphic units of TSK-3 (gneisses) and TSK-7 (trondhjemites) studied by Galoyan et al. (2020) are also shown.

reactions were $(2.64 \pm 0.02) \cdot 10^{-4}$ for $(^{36}Ar/^{37}Ar)_{Ca}$, $(6.73 \pm 0.04) \cdot 10^{-4}$ for $(^{39}Ar/^{37}Ar)_{Ca}$, $(1.21 \pm 0.003) \cdot 10^{-2}$ for $(^{38}Ar/^{39}Ar)_K$ and $(8.6 \pm 0.7) \cdot 10^{-4}$ for $(^{40}Ar/^{39}Ar)_K$. All errors are quoted at the 2σ level and include all analytical errors. All relevant analytical data for age calculations can be found in the Supplementary Data S5.

5. Results

5.1. Metamorphic basement rocks

Descriptions and mineral contents of the SAB metamorphic basement rock samples are given in Table 1. Detailed petrographic observations of the rocks, as well as their isotope, major and trace element geochemistry, are provided in Supplementary Data S2 and S3, respectively. Two of the samples, TSK-3 and TSK-7, represent igneous intrusive bodies that penetrated the basement of the SAB.

Granite gneiss sample TSK-3 has a trace element geochemistry typical for granites formed in active continental margins (Fig. 5a) (Schandl and Gorton, 2002) and volcanic arcs (Fig. 5b-c) (Pearce et al., 1984). It also has compositional similarities with Neoproterozoic–Early Cambrian (541–547 Ma) subduction-related granitoids and metamorphic rocks from Iran studied by Balaghi Einalou et al. (2014) (Fig. 5), which constitute part of the crystalline basement underlying the Sanandaj–Sirjan zone, Central Iran and the Alborz Mountains (Hassanzadeh et al., 2008).

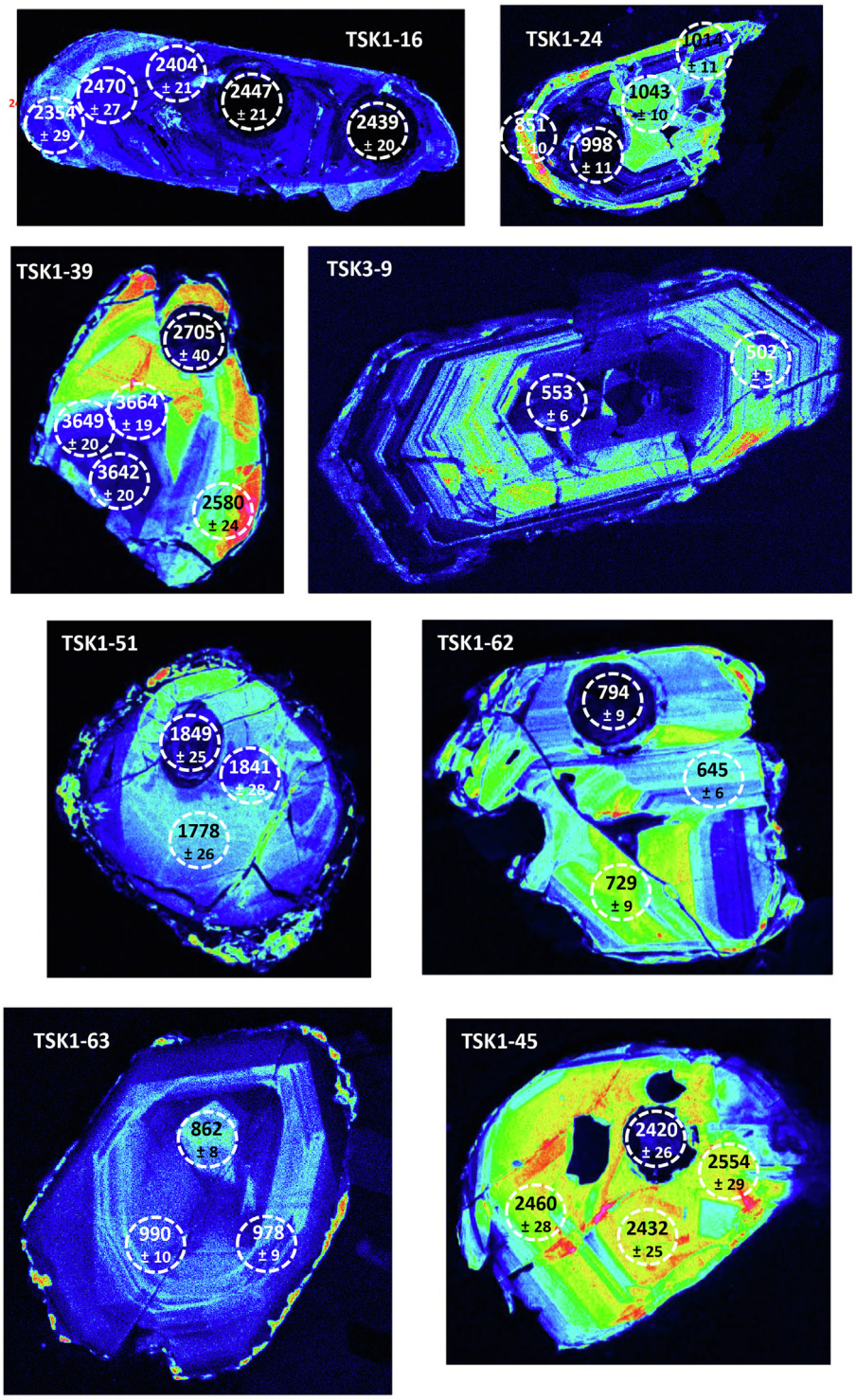

Fig. 6. Cathodoluminescence images of representative zircons used for U-Pb dating and trace-element analysis. Samples are TSK1-16, TSK1-24, TSK1-39, TSK3-9, TSK1-51, TSK1-62, TSK1-63, and TSK1-45. Dashed circles denote the analysed spots for LA-ICP-MS U-Pb dating (sized 20–40 μm). Numbers are the determined ages in Ma ($^{238}U/^{206}Pb$ ages for zircons younger than 1.0 Ga, $^{207}Pb/^{206}Pb$ ages for older zircons). Uncertainties are given at the 2σ level.

Trondhjemite ("plagiogranite") sample TSK-7, which is composed of euhedral plagioclase (60–75%) and quartz (25–40%), represents a suite of metamorphosed leucrocratic intrusions in the SAB basement (Fig. 2). The metamorphic grade of these trondhjemites is low compared to the surrounding amphibolites and metapelite mica schists, as evidenced by the degree of preservation of primary magmatic zoned plagioclases and the absence of schistosity. A silica–total alkali classification (after Cox et al., 1979) confirms its granitic nature, and its trace-element content plots in the field of arc granites (Fig. 5b-c) (Pearce et al., 1984). The high Sr/Y ratio (234) at low Y (1.3 ppm) indicates an affinity with adakite/TTG rocks (Fig. 5d) (Defant and Drummond, 1990).

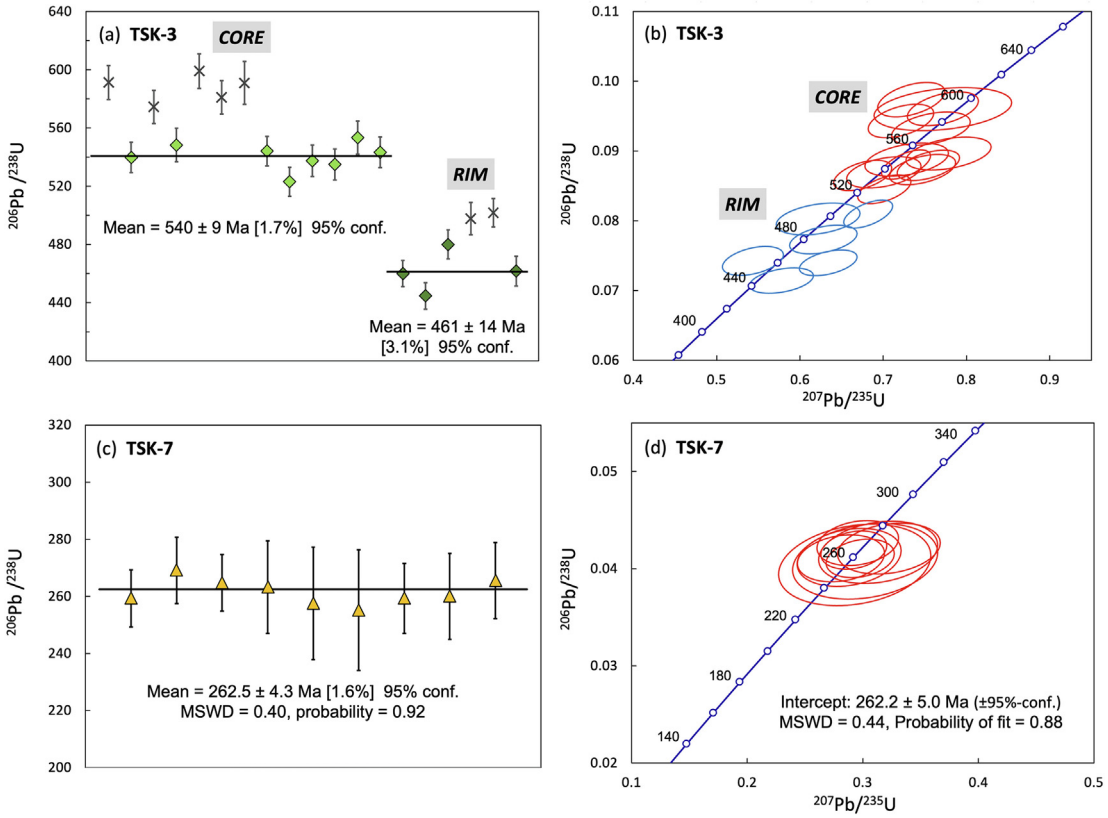

Fig. 7. (a,c) Weighted average by data-point errors for the metamorphosed intrusions in the basement of the SAB (TSK-3, TSK-7); (b,d) U-Pb concordia plots ($^{207}Pb/^{235}U$ vs. $^{206}Pb/^{238}U$). Crosses denote discordant data, which were excluded from weighted mean age calculations. Data-point error symbols and ellipses are 2σ.

5.1.1. Zircon geochronology and geochemistry

A total of 130 spots on 58 zircon grains from samples TSK-1,3,5,7 was analysed for U-Pb ages by LA-ICP-MS (Supplementary Data S3 and S4). Back-scattered electron (BSE) and transmitted light images of representative zircons are shown in Fig. 6. The results for magmatic samples (TSK-3 and TSK-7) are plotted on weighted average (WA) and concordia diagrams (Fig. 7). For detrital samples (TSK-1 and TSK-5), the results are presented on probability/density plots in Fig. 8 (with all uncertainties are given at the 2σ level). In the following discussion, U-Pb ($^{238}U/^{206}Pb$) ages are used for zircons younger than 1.0 Ga, and Pb-Pb ($^{207}Pb/^{206}Pb$) ages are used for older zircons.

The U-Pb zircon ages for granite gneiss sample TSK-3 spread along the concordia from ~ 600 to 440 Ma (Fig. 7). Core ages range from 600 to 520 Ma (WA = 540 ± 9 Ma), whereas rim ages range from 520 to 440 Ma (WA = 461 ± 14 Ma). The probability–density diagram (not shown) shows a peak at ~540 Ma for the zircon cores. This age is defined by the most concordant (98–102%) zircons, suggesting that this is the age of granite formation.

The U-Pb zircon ages for trondhjemite sample TSK-7 yield a WA age of 262.5 ± 4.3 Ma (Fig. 7c) and concordia intercept of 262.2 ± 5.0 Ma (Fig. 7d). The former is taken as the intrusion age.

Mica schist TSK-1 and metaarkose phyllite TSK-5 are host to a substantial number of detrital zircons. U-Pb and Pb-Pb zircon ages show considerable variability, ranging from 3,650 Ma to 86 Ma (Fig. 8). These zircons can be divided into 5 age groups. Remarkably, the core of one grain from TSK-1 yields Eoarchean (3,650 Ma) ages (photo in Fig. 6). A Neoarchean-Palaeoproterozoic group comprising mostly TSK-1 zircons and one TSK-5 zircon, defines an age peak at ~ 2,500 Ma. Another Palaeoproterozoic group (1,655–1,850 Ma) is observed, consisting only of TSK-1 zircons, as is a Meso-Neoproterozoic group at 970–1,040 Ma. The majority of the zircons, both from TSK-1 and TSK-5, constitute a Neoproterozoic group, ranging from 527 to 850 Ma. This group defines a marked peak at ~600 Ma. TSK-1 also hosts a few Cretaceous (86–120 Ma) zircons.

All zircon grains were analysed for trace elements by LA-ICP-MS (Supplementary Data S3 and S4). Virtually all zircons have Th/U ratios between 0.3 and 1 (Fig. 9a), indicative of magmatic zircons (Teipel et al., 2004 and references therein). The overall range in Y content versus U/Yb ratios plot entirely within the field of continent-derived zircons (Grimes et al., 2007) and predominantly within that of continental granitoids (Fig. 9b) (Ballard et al., 2002; Belousova et al., 2006). Rare-earth element concentrations for zircons, normalised to C1 chondrite (McDonough and Sun, 1995), are typical of growth under magmatic conditions, with TSK-3 and TSK-1,5 showing minor negative Eu anomalies (Fig. 9c,d). TSK-7 has no negative Eu anomaly. They collectively indicate HREE enrichment up to about 5,000 times C1 chondrite, with marked HREE fractionation ($Yb_N/Gd_N > 1$).

5.2. Mafic to intermediate sills and dykes

5.2.1. Elemental and isotope geochemistry

The studied sills at Khor Virap and Arpi are predominantly basaltic rocks that are mildly alkaline to sub-alkaline (Fig. 10a) (Le Bas et al., 1986) with SiO_2 contents ranging from 47.7 to 50.5 wt%. Detailed petrographic observations are listed in Supplementary Data S2. Conversely, dyke sample ARP-3 and ARP-5 classify as andesites (SiO_2 = 61.0–61.3 wt%). All samples are calc-alkaline (Peccerillo and Taylor, 1976) and have relatively low K_2O content, ranging from 0.4 to 1.6 wt%. MgO content is moderate (3.7–8.2 wt%), with samples showing variable Mg-numbers [44–

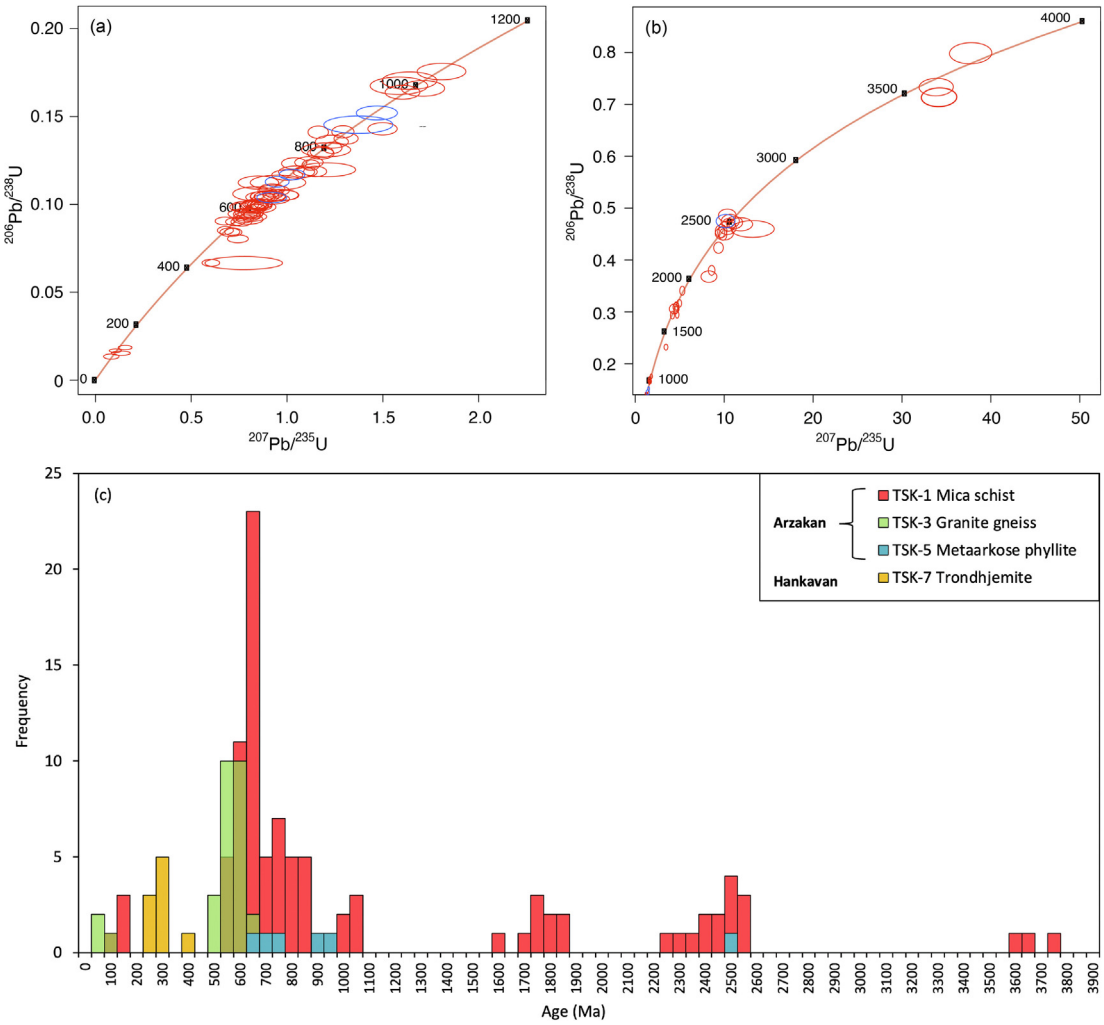

Fig. 8. (a,b) U-Pb concordia plots ($^{207}Pb/^{235}U$ vs. $^{206}Pb/^{238}U$) for zircons from the metamorphic basement rocks (TSK-1, TSK-5). Data-point error symbols are 2σ. (c) Histogram of zircon ages from metamorphic basement rocks TSK-1,3,5,7.

55; Mg# = 100 × Mg/(Mg + Fe^{2+})]. Andesites ARP-3 and ARP-5 are further marked by lower FeO_{tot} (6.0 vs. 11.5–12.1 wt%, respectively), CaO (5.4–5.8 vs. 8.0–12.5 wt%) and TiO_2 contents (0.8–0.9 vs. 1.8–2.9 wt%). The basalts, with the exception of sample KV-2, show enrichments in virtually all incompatible trace elements, with high LILE, HFSE and LREE abundances and relatively low LILE/HFSE values (e.g., Ba/Nb = 6–12). Primitive mantle-normalised incompatible trace element patterns (Fig. 10c-d) indicate that the main group of basalts from both sections closely resemble typical OIB. Although the three Arpi sills show patterns almost identical to the OIB-like Khor Virap samples, they have slight negative Pb anomalies (Pb/Pb* = 0.4–0.7). In contrast, the pattern for sample KV-2 is flatter, characterised by lower incompatible trace-element abundances, including LREE, LILE and HFSE, and displays a positive Pb anomaly (Pb/Pb* = 1.7; Fig. 10d). It is marked by lower LREE/HREE than OIB-type compositions (e.g., La/Yb = 5.9 vs. 9.8–13.5), as well as slightly higher LILE/HFSE (e.g., Ba/Nb = 14.6 vs. 6–12). It shows a clear affinity with typical P-MORB compositions (e.g., Schilling et al., 1983; Saccani et al., 2013b, 2014), except for slightly lower Nb, Ta, and Sr contents.

Andesites ARP-3 and ARP-5 collectively have different primitive mantle-normalised patterns (Fig. 10c) and are relatively enriched in the most incompatible trace elements. They show patterns similar to P-MORB, except for substantial negative Nb-Ta and Ti anomalies, slight positive Th and U anomalies and higher contents in several LILE (e.g., Ba, Rb, Cs), and can therefore be classified as subduction-related.

Sr-Nd-Pb isotope compositions of samples KV-1, KV-2, ARP-1, ARP-3 and ARP-4 are shown in Fig. 10e-f (and listed in Supplementary Data S3). Age-corrected values were calculated using the age data from the same samples (next section). Arpi rocks show restricted $(^{87}Sr/^{86}Sr)_i$ values, ranging from 0.70452 to 0.70511, whereas Khor Virap basalts have slightly higher values (0.70535–0.70642). The highest value corresponds to KV-2, which also shows a distinct trace elemental composition (P-MORB affinity).

5.2.2. $^{40}Ar/^{39}Ar$ geochronology

The results of the $^{40}Ar/^{39}Ar$ dating for samples KV-1 (OIB), KV-2 (P-MORB), ARP-3 (andesite), and ARP-4 (OIB) are shown in Fig. 11, listed in Table 2 and Supplementary Data S5.

Two replicate heating experiments of amphibole KV-1 (VU109-I3) were performed. The first sample (VU109-I3_1) yields a "plateau" age of 188.5 ± 1.1 Ma (Fig. 11a) for the steps with higher radiogenic yields (>59%), but contains only 29.1% of the $^{39}Ar_K$ released. The atmospheric isochron intercept overlaps with air at 2σ (289.0 ± 10.3). The majority of the individual heating steps in the full age spectrum range between 169 and 189 Ma. The second experiment (VU109-I3_2) yields a "plateau" of 187.3 ± 0.8 Ma for the middle part of the heating spectrum ($^{39}Ar_K$ = 40.1%; MSWD = 2.7). The inverse isochron age is identical at 188.4 ± 1.4 Ma with an

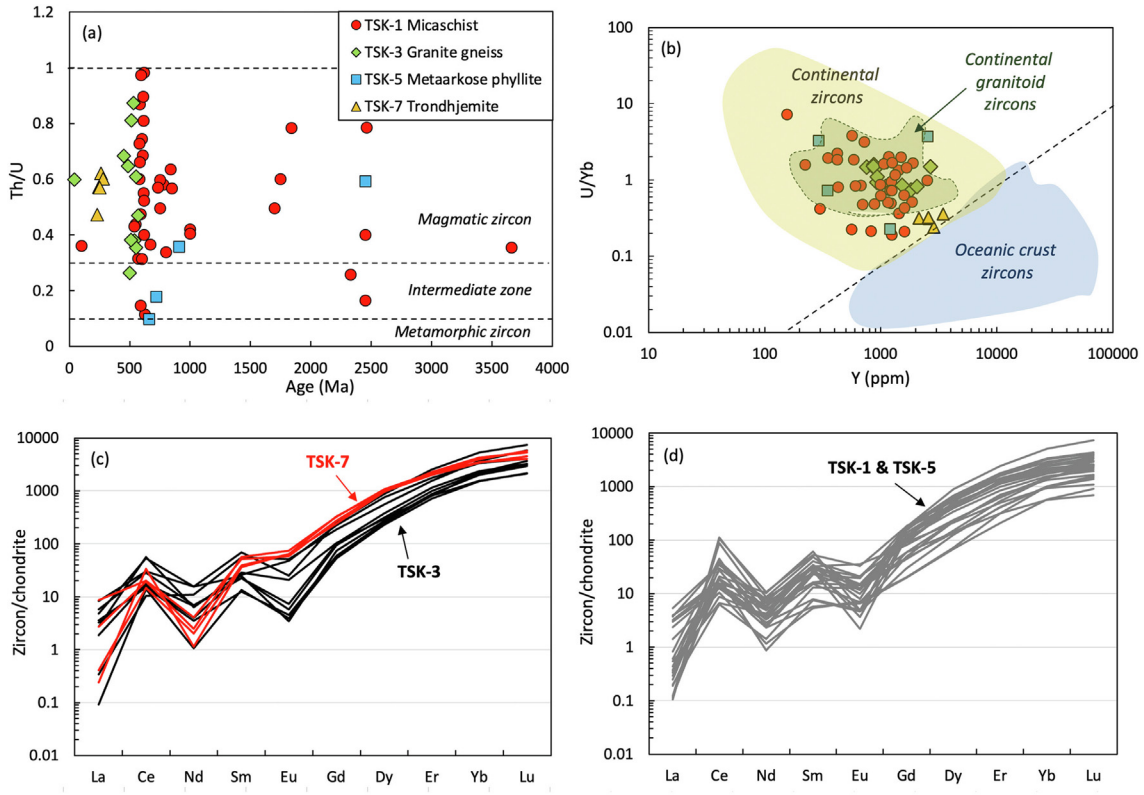

Fig. 9. Zircon trace-element composition diagrams for samples TSK-1 (micaschist), TSK-3 (granite gneiss), TSK-5 (metaarkose phyllite), and TSK-7 (trondhjemite). (a) Zircon age (Ma) versus Th/U. Note that the majority of the grains originates from magmatic sources. Zircon fields are from Teipel et al. (2004) and references therein. (b) Y (ppm) versus U/Yb. Coloured fields indicate the compositional range of zircons derived from oceanic crust (blue), continent (yellow) (Grimes et al., 2007) and continental granitoids (green) (Ballard et al., 2002; Belousova et al., 2006). Note that all zircons are continent-derived. Rare-earth element concentrations for (c) magmatic (TSK-3, TSK-7) and (d) detrital zircons (TSK-1, TSK-5) normalised to C1 chondrite (McDonough and Sun, 1995). (For interpretation of the references to colour in this figure legend, the reader is referred to the web version of this article.)

$^{40}Ar/^{36}Ar$ intercept of 292.5 ± 7.3. The two experiments are remarkably similar. Although not formally fulfilling definition of a plateau age (a.o., comprising > 50% $^{39}Ar_K$ released), the "plateau" age of 188.5 ± 1.1 Ma most probably represents the eruption age.

Two replicate heating experiments of plagioclase sample KV-2 (VU118-I1) show disturbed age spectra with ages starting from ~110 Ma, increasing to ~245 Ma (I1a) and ~250 Ma (I1b) and decreasing to ~185 Ma. Note that the initial age step of ~110 Ma is remarkably close to the magmatic event observable in the Arpi area (samples ARP-3 and ARP-5) and Darasham (Khanzatian, 1992). The preferred age is 233.7 ± 5.1 Ma (Fig. 11b), comprising 52.9% of the total $^{39}Ar_K$.

For plagioclase of sample ARP-3 (VU109-I4) one incremental heating experiment was performed. The sample shows a decreasing age spectrum. Six consecutive lower temperature heating steps yield a weighted mean age of 124.5 ± 0.5 Ma, comprising only 18.5% of the total $^{39}Ar_K$. Four consecutive higher temperature heating steps seem to define a "plateau" of 112.8 ± 0.5 Ma (Fig. 11c; comprising 28.9% $^{39}Ar_K$) with an atmospheric $^{40}Ar/^{36}Ar$ intercept (296.3 ± 9.5). This result is in good agreement with the U-Pb zircon ages of 116.7 ± 1.5 Ma for ARP-3 and 115.0 ± 1.4 Ma for ARP-5.

Two incremental heating experiments were performed on the groundmass of sample ARP-4 (VU109-I5). The first experiment did not result in a reliable plateau, but shows an increase in age followed by a decrease from ~80 Ma to ~230 Ma to ~210 Ma. The second experiment shows similar behaviour, resulting in ages from ~83 Ma to ~247 Ma to ~218 Ma. Note that the initial heating steps of 85 Ma are remarkably close to the SAB ophiolite obduction age (Rolland et al., 2009; Hässig et al., 2016a, 2016b, 2017, Rolland et al., 2020). The radiogenic yields are high and an isochron could not be defined due to clustering of data points. Weighted mean ages of the four oldest consecutive steps yielded 230.9 ± 1.5 Ma (MSWD = 35.9; $^{39}Ar_K$ = 34.0%, $^{40}Ar^*$ = 88.6%; K/Ca = 0.116 ± 0.007) and 245.4 ± 1.4 Ma (Fig. 11d; MSWD = 7.4; $^{39}Ar_K$ = 28.5%, $^{40}Ar^*$ = 88.4%; K/Ca = 0.143 ± 0.011), respectively. The latter age is preferred and is in remarkable agreement with the U-Pb zircon age of 246.0 ± 3.3 Ma for ARP-1.

5.2.3. Zircon geochronology

In addition to $^{40}Ar/^{39}Ar$ dating, samples containing zircons were also U-Pb dated, considering the altered nature of the samples studied. A total of 35 zircon grains from samples ARP-1,3,4,5 and KV-1,2,3 were analysed for U-Pb ages by LA-ICP-MS (Supplementary Data S3). The results for ARP-1,3,5 are reported in concordia diagrams and weighted average (WA) plots (Fig. 12). The mean U-Pb zircon age is 246.0 ± 3.3 Ma for ARP-1; 116.7 ± 1.5 Ma for ARP-3; and 115.0 ± 1.4 Ma for ARP-5. The age for ARP-3 is in good agreement with the $^{40}Ar/^{39}Ar$ plateau age of 112.8 ± 0.5 Ma. The zircons in this sample were also analysed for trace elements by LA-ICP-MS (Supplementary Data S3).

Samples KV-1,2,3 and ARP-1,4 also contain zircons that are marked by U-Pb ages ranging from about 440 to 1,848 Ma (Supplementary Data S3), far exceeding the $^{40}Ar/^{39}Ar$ ages of their host rocks as well as the age of the sediments that host the intrusions. They show remarkable overlap with the metamorphic basement zircons on a density/probability plot (Supplementary Fig. S2) and

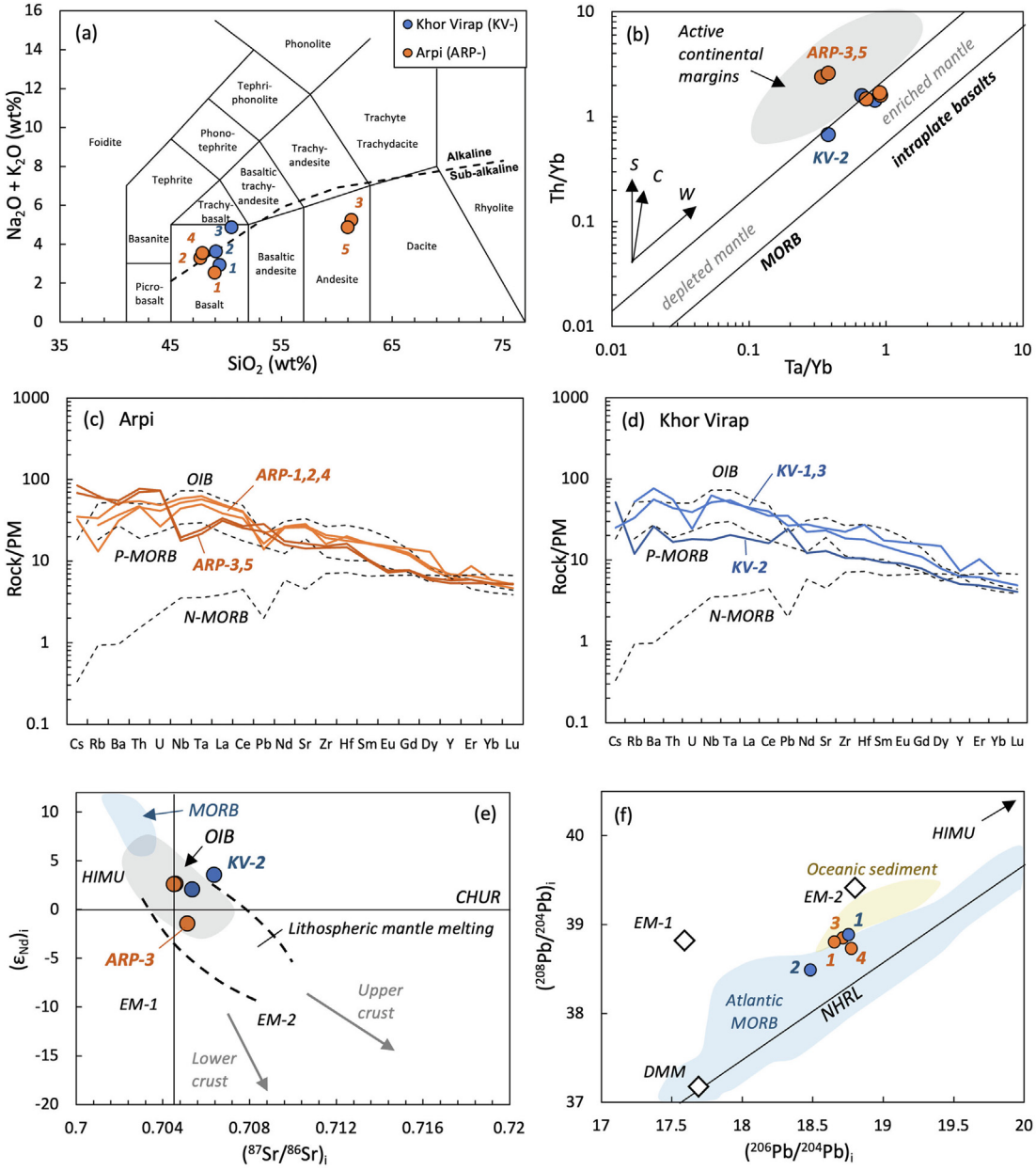

Fig. 10. Elemental and Sr-Nd-Pb isotope compositions of the Armenian intrusions. (a) SiO_2 vs. total alkali ($Na_2O + K_2O$) classification diagram (Le Bas et al., 1986). Boundary between alkaline and sub-alkaline fields after Miyashiro (1978). (b) Ta/Yb vs. Th/Yb discrimination diagram (Pearce, 1982), illustrating the MORB-OIB mantle array. S = subduction zone enrichment trend; C = crustal contamination trend; W = within-plate enrichment trend. Primitive mantle–normalised (McDonough and Sun, 1995) incompatible trace-element diagrams for (c) Arpi and (d) Khor Virap intrusions. (e) $(^{87}Sr/^{86}Sr)_i$ vs. $(\varepsilon_{Nd})_i$ and (f) $(^{206}Pb/^{204}Pb)_i$ versus $(^{208}Pb/^{204}Pb)_i$. Plotted for comparison are the NHRL (Northern hemisphere reference line; Hart, 1984), oceanic sediments (Othman et al., 1989), HIMU, EM-1, and EM-2 (Zindler and Hart, 1986; Hart et al., 1992) and Atlantic MORB (Agranier et al., 2005; Hoernle et al., 2011). Where relevant, N-MORB, E-MORB, OIB (Sun and McDonough, 1989), HIMU, EM-1 and EM-2 (Willbold and Stracke, 2006) and P-MORB (Saccani et al., 2013b, 2014) are shown for comparison.

can therefore be considered as being "xenogenic", i.e., entrained during magma ascent.

6. Discussion

6.1. NE Gondwanan margin: Origin of the SAB

The *peri*-Gondwanan origin of SAB has long been inferred on the basis of its Cadomian–Neoproterozoic basement ages (Knipper and Khain, 1980; Aghamalyan, 1998, 2004) and is central to recent geodynamic interpretations (e.g., Meijers et al., 2015; Rolland, 2017; van Hinsbergen et al., 2020). Here, for the first time, the detrital (TSK-1, TSK-5) and magmatic (TSK-3) zircon record preserved in the metamorphic basement of the SAB (Figs. 1 and 2) provides insight into the palaeo-position of the SAB. Fig. 13 presents histograms of compiled ages from Late Neoproterozoic–Cenozoic detrital zircons derived from basements of the SAB (this study), the Taurides, Sakarya, Pontides, and Iran. This comparison demonstrates a marked similarity between the Neoproterozoic–Palaeozoic detrital zircon ages (TSK-1, TSK-5) and those of the neighbouring terranes, which firmly establishes a Gondwanan origin for the SAB. The widespread overlap of various age groups within the zircon record do not, at present, seem to allow a more precise palaeo-position of the SAB to be established for (pre-)Gondwanan times.

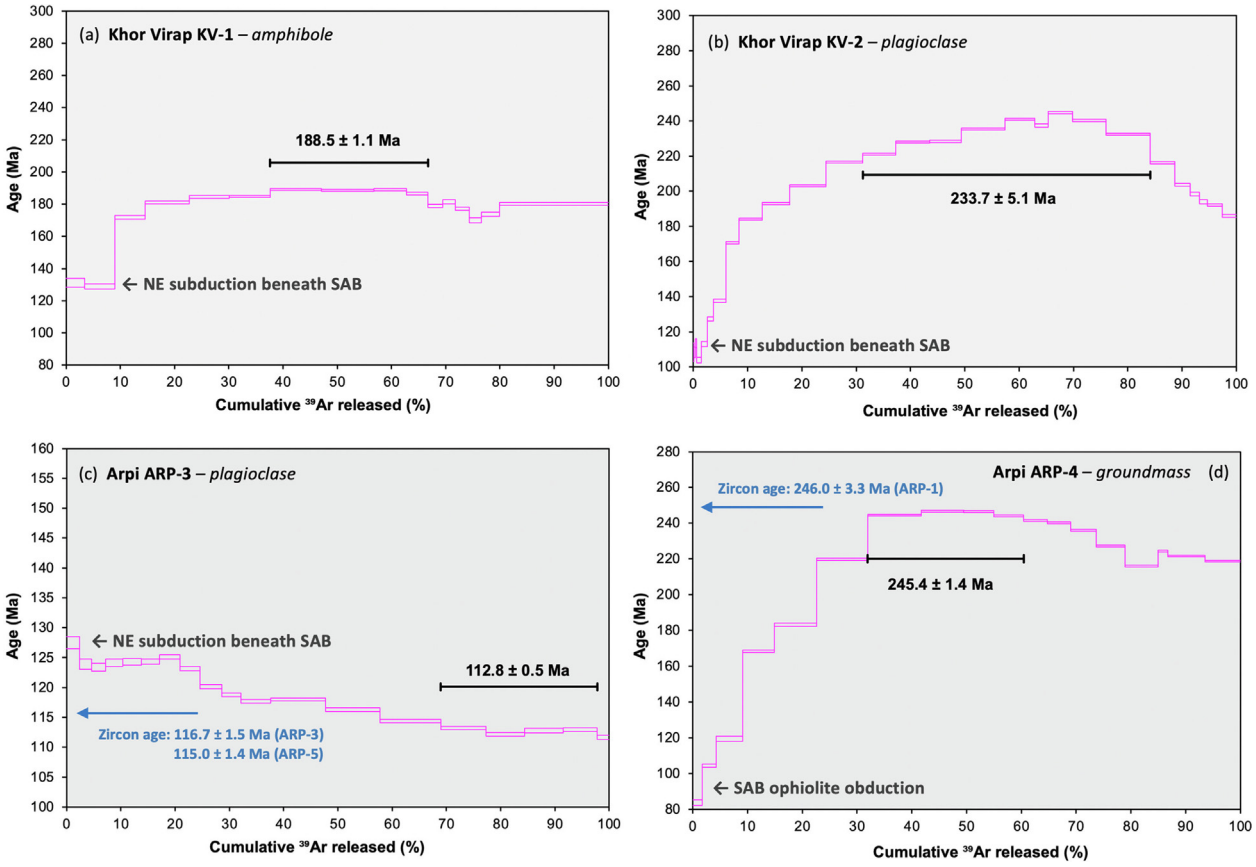

Fig. 11. Results of $^{40}Ar/^{39}Ar$ incremental heating experiments for samples (a) KV-1 (amphibole), (b) KV-2 (plagioclase), (c) ARP-3 (plagioclase), and (d) ARP-4 (groundmass). Weighted mean ("plateau") ages are reported with 2σ analytical uncertainty. Corresponding zircon ages from this study are indicated in (c) and (d). The ages of relevant large-scale tectonic events are also indicated. Detailed analytical data are provided in Supplementary Data S5.

Table 2
Summary of $^{40}Ar/^{39}Ar$ results. MSWD = mean square weighted deviate; N = number of steps included (excluded) in the plateau age; $^{39}Ar_K$ (%) = percentage of $^{39}Ar_K$ released by plateau steps. Uncertainties are given at the 2σ level. Ages in bold face are the preferred ages. Detailed analytical data are provided in Supplementary Data S5.

Sample	Irradiation ID	Material	Weighted mean age (Ma)	MSWD	$^{39}Ar_K$ (%)	$^{40}Ar^*$ (%)	K/Ca	N	Inverse isochron age (Ma)
KV-1	VU109-I3_1	amphibole	**188.5 ± 1.1**	2.5	29.1	68.4	0.074	4(12)	289.0 ± 10.3
KV-1	VU109-I3_2	amphibole	187.3 ± 0.8	2.7	40.1	73.7	0.059	6(8)	292.5 ± 7.3
KV-2	VU118-I1a	plagioclase	**233.7 ± 5.1**	635.2	52.9	96.4	0.296	9(18)	360.7 ± 58.1
KV-2	VU118-I1b	plagioclase	236.5 ± 8.3	1248.5	38.0	95.9	0.320	7(17)	291.9 ± 39.6
ARP-3	VU109-I4_1	plagioclase	124.5 ± 0.5	1.3	18.5	50.4	0.223	6(13)	296.0 ± 2.5
ARP-3	VU109-I4_1	plagioclase	**112.8 ± 0.5**	2.1	28.9	68.1	0.076	4(15)	296.3 ± 9.5
ARP-4	VU109-I5_1	groundmass	230.9 ± 1.5	35.9	34.0	88.6	0.116	4(13)	266.4 ± 193.6
ARP-4	VU109-I5_2	groundmass	**245.4 ± 1.4**	7.4	28.5	88.4	0.143	4(14)	222.7 ± 123.7

Most of these Gondwana-derived terranes contain evidence for Late Ediacaran–Early Cambrian magmatism, thought to be associated with a widespread continental arc along the northern margin of newly-formed Gondwana (Gessner et al., 2001; Ramezani and Tucker, 2003; Hassanzadeh et al., 2008). Evidence for this magmatism is found in the neighbouring terranes of Central Iran, where Neoproterozoic magmatic products have been found in the basement (Ramezani and Tucker, 2003; Hassanzadeh et al., 2008), and the Menderes massif of the Anatolide-Tauride platform, where active-margin type granites of Ediacaran-Cambrian age are exposed (Gessner et al., 2001). The magmatic zircons of mica granite-gneiss TSK-3, a metamorphosed intrusion into the SAB basement (Fig. 8), is consistent with this extensive magmatic episode in Ediacaran–Early Cambrian times. Its whole-rock composition is similar to typical volcanic arc granites and suggests formation in an active continental margin (Fig. 5).

6.2. Cimmerian continent: Rift initiation in the SAB

The Cimmerian continent was originally coined by Şengör and Yilmaz (1981) as an arc ripped from the NE margin of Gondwana above a SW-dipping Palaeotethys subduction zone in Late Permian–Early Triassic times. Recent evidence suggests that the opening of the Neotethys might have occurred as a result of back-arc spreading (Şengör et al., 2019b), as opposed to Atlantic-type continental margins on both sides of the Cimmerian continental ribbon. Since its original discovery, a substantial amount of Permian–Triassic rift-related magmatism has been identified along the collision belt, from Iran to China (e.g., Lapierre et al., 2004, 2007; Chauvet et al., 2008; Shellnutt et al., 2014; Shakerardakani et al., 2018; Wang et al., 2019; Zeng et al., 2019). The north-westernmost end of this continental ribbon appears to lie east of the Taurides (NE Turkey), as there Cretaceous ophiolites are found overthrusted by

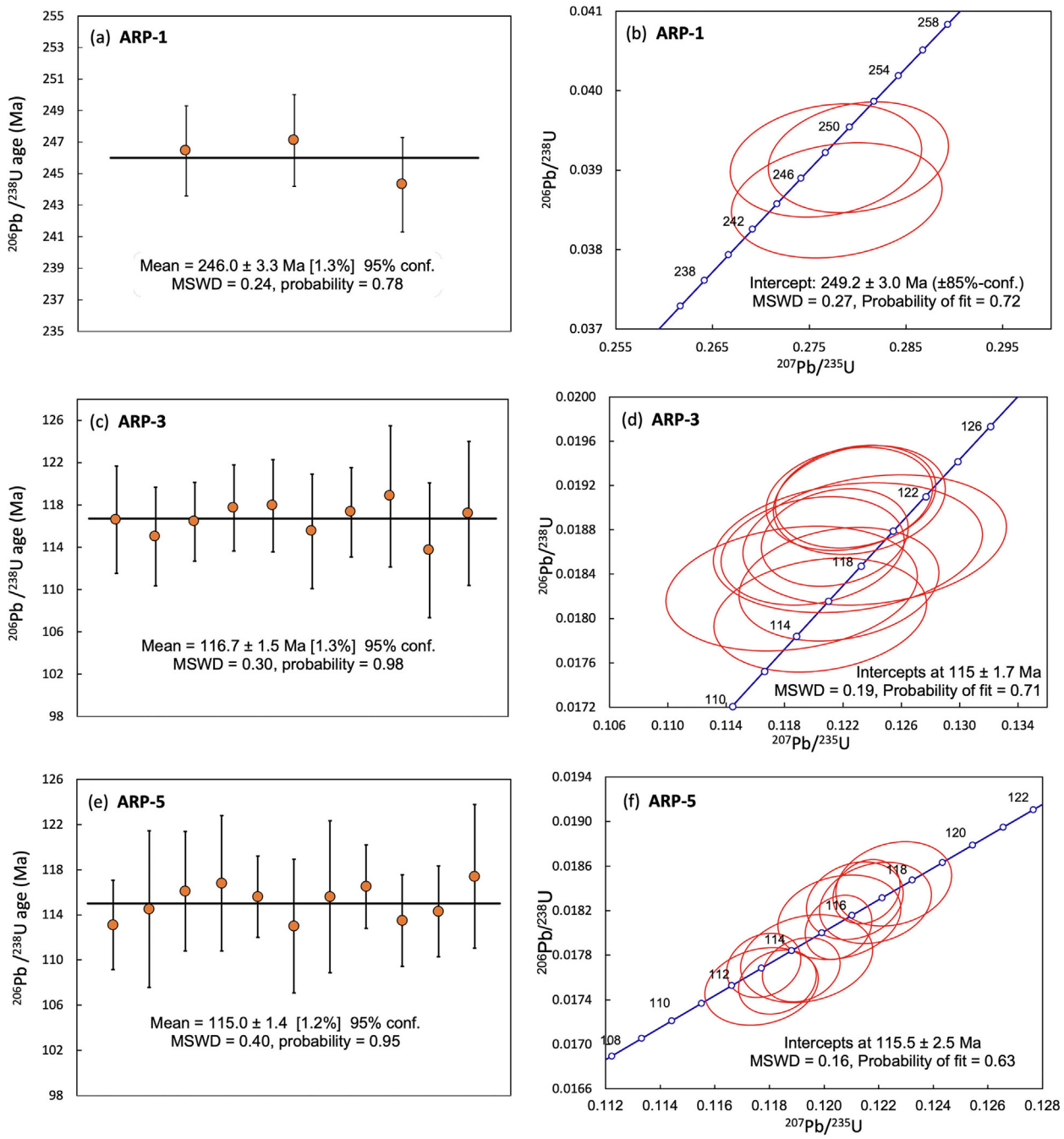

Fig. 12. (a,c,e) Weighted mean $^{206}Pb/^{238}U$ age by data-point errors for the mafic to intermediate intrusions in the sedimentary cover of the SAB at Arpi (ARP-1, ARP-3, ARP-5). (b,d,f) U-Pb concordia plots ($^{207}Pb/^{235}U$ vs. $^{206}Pb/^{238}U$). Data-point error symbols and ellipses are 2σ.

Jurassic ophiolites of the southern Pontide margin during the Cenozoic (Topuz et al., 2013b).

Details on the movement of the SAB within the Tethyan realm after its separation from Gondwana are lacking except for a single palaeomagnetic study on volcanics in southern Nakhichevan (Bazhenov et al., 1996), which positioned the SAB (21.4°N ± 3.7°) at the African margin around the Early Jurassic, founded on results from four sites yielding positive fold and conglomerate tests, and a rock age inferred from geological mapping and stratigraphic relationships with sediment suites. Limestones and dolomites in the Julfa area, thought to be Middle-Upper Triassic (Karyakin, 1989), have later turned out to be Lower Triassic based on fossil fauna (Grigoryan, 1990). These rocks are overlain discordantly by presumed Lower Jurassic (devoid of any fossil fauna) and Middle Jurassic sedimentary sequences (Azizbekov, 1962; Grachev and Karyakin, 1983). This revised stratigraphic interpretation implies that the volcanics studied by Bazhenov et al. (1996) can be any age between 247 and 174 Ma. The uncertainty questions the robustness of earlier geodynamic reconstructions, which have often relied on this single palaeomagnetic constraint. Due to the lack of local geological evidence, existing geodynamic views for the Mesozoic rifting evolution of the SAB often depend on an assumed association with a neighbouring terrane. One group considers the SAB to be a contiguous part of the Anatolide-Taurides block, which did not start rifting until the Early Jurassic (e.g., Okay and Tüysüz, 1999; Barrier and Vrielynck, 2008; Rolland

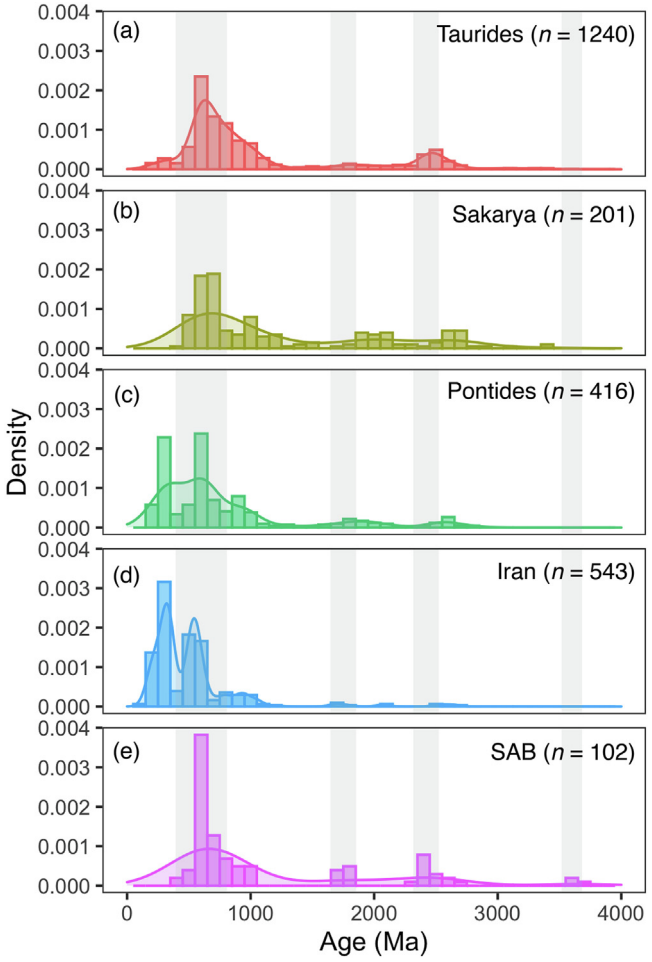

Fig. 13. Histogram and smoothed density estimates of zircon ages of the metamorphic basement of (a) the Taurides (Menderes massif; Abbo et al., 2015), (b) Sakarya (Aysal et al., 2012; Ustaömer et al., 2012), (c) Pontides (Ustaömer et al., 2013; Okay et al., 2014), (d) Central Iran (incl., Sanandaj-Sirjan zone; Fergusson et al., 2016; Chiu et al., 2017), and (e) the SAB (this study; detrital zircons from samples TSK-1,5).

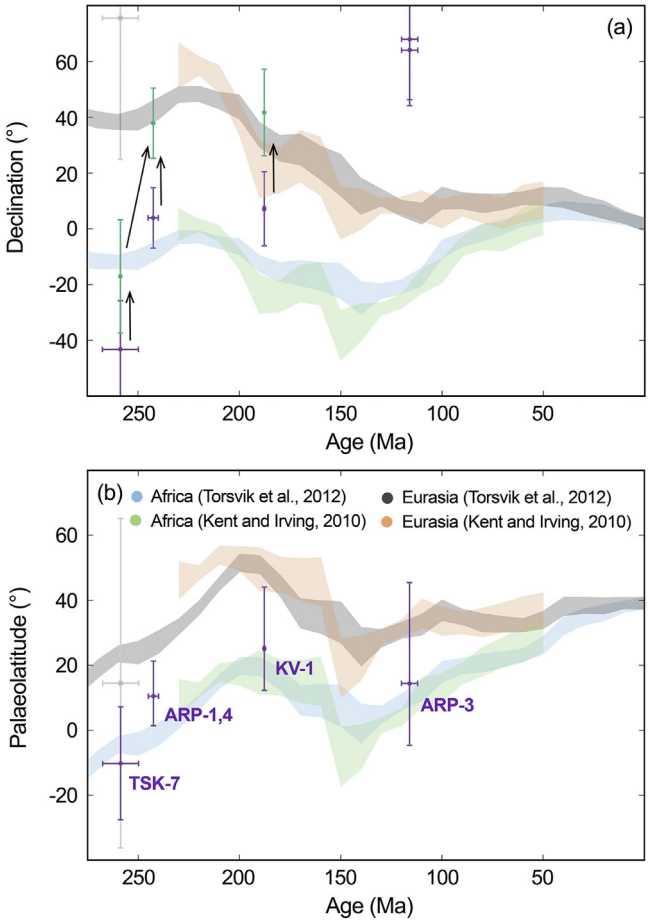

Fig. 14. Plots of age (in Ma) versus (a) mean declination and (b) palaeolatitude for the investigated SAB sites (Supplementary Data S1). Shaded areas show the respective values based on the apparent polar wander paths of Kent and Irving (2010) and Torsvik et al. (2012). Grey data shows the secondary component of TSK-7. Black arrows and green data points show restored vertical axis rotation related to the counterclockwise rotation of the SAB (see section 6.2 for further explanation). (For interpretation of the references to colour in this figure legend, the reader is referred to the web version of this article.)

et al., 2012; Rolland, 2017). Another group links it to Central Iran (e.g., Stampfli et al., 1991; Brunet et al., 2003; Adamia et al., 2017), which began to drift northward in Early Permian times as part of the Cimmerian blocks and reached Eurasia during the Late Triassic (Zanchi et al., 2009, and references therein). More recently, the SAB has been interpreted as an isolated microcontinent that, together with the Pontides, drifted away from the Taurides during the Triassic (van Hinsbergen et al., 2020).

6.2.1. Middle–Late Permian trondhjemite intrusions at Tsakhkunyats

The trondhjemite ("plagiogranite") intruded into the previously-metamorphosed basement of the SAB at 262.5 ± 4.3 M a. Based on the same Middle–Late Permian trondhjemite suite, Galoyan et al. (2020) surmised the existence of a long-lived S-dipping subduction zone by linking the petrogenesis of these rocks to the Carboniferous subduction zone that generated metagranites in the Afyon zone in western Turkey (Candan et al., 2016), though it is unclear whether the disparate occurrences are related. Our palaeomagnetic data for this sample (Supplementary Data S1) point to a position at the NE margin of Gondwana at this time, next to the Pontides and the Iranian blocks (Fig. 14b). Its geochemical signature (Fig. 5) suggests magma genesis in an active continental margin. The trondhjemite is characterised by significant enrichment in Na over K (Na_2O/K_2O = 7), relatively high Sr (302 ppm), low Y (1.3 ppm) and Yb (0.2 ppm) and high Sr/Y (234), similar to adakitic melts. High Na_2O/K_2O ratios and incompatible-element patterns of the studied sample, as well as of samples from the same trondhjemite suite reported by Galoyan et al. (2020), more closely resemble modern subduction-related adakites and are different from thickened lower continental crust-derived adakites based on $(La/Yb)_N$ vs. $(Ba/Zr)_N$ (Fig. 5e). Sr-Nd isotope systematics (Fig. 5f) further demonstrate the affinity of the Tsakhkunyats trondhjemites to compositional fields of subduction-derived adakites, rather than lower continental crust adakites.

Middle–Late Permian volcanic arc-type intrusions into the SAB imply an active SW-dipping subduction at the NE margin of Gondwana at that time, whereby the SAB was part of the overriding plate (Fig. 15). This inference is in good agreement with recent evidence of the presence of arcs recorded as Upper Permian–Lower Triassic rocks across the Cimmerian continent, which became dispersed during the Alpine evolution (Şengör et al., 2019a). Similar Upper Permian–Lower Triassic arc-related rocks have been documented for the Pontides and Sakarya Zone (e.g., Eyuboglu et al., 2011; Karsli et al., 2016; Topuz et al., 2018), but are absent in the Anatolide-Tauride block. This observation corroborates the palaeo-position of the SAB as the SE extension of the Pontides during the Gondwanan assembly (Fig. 15).

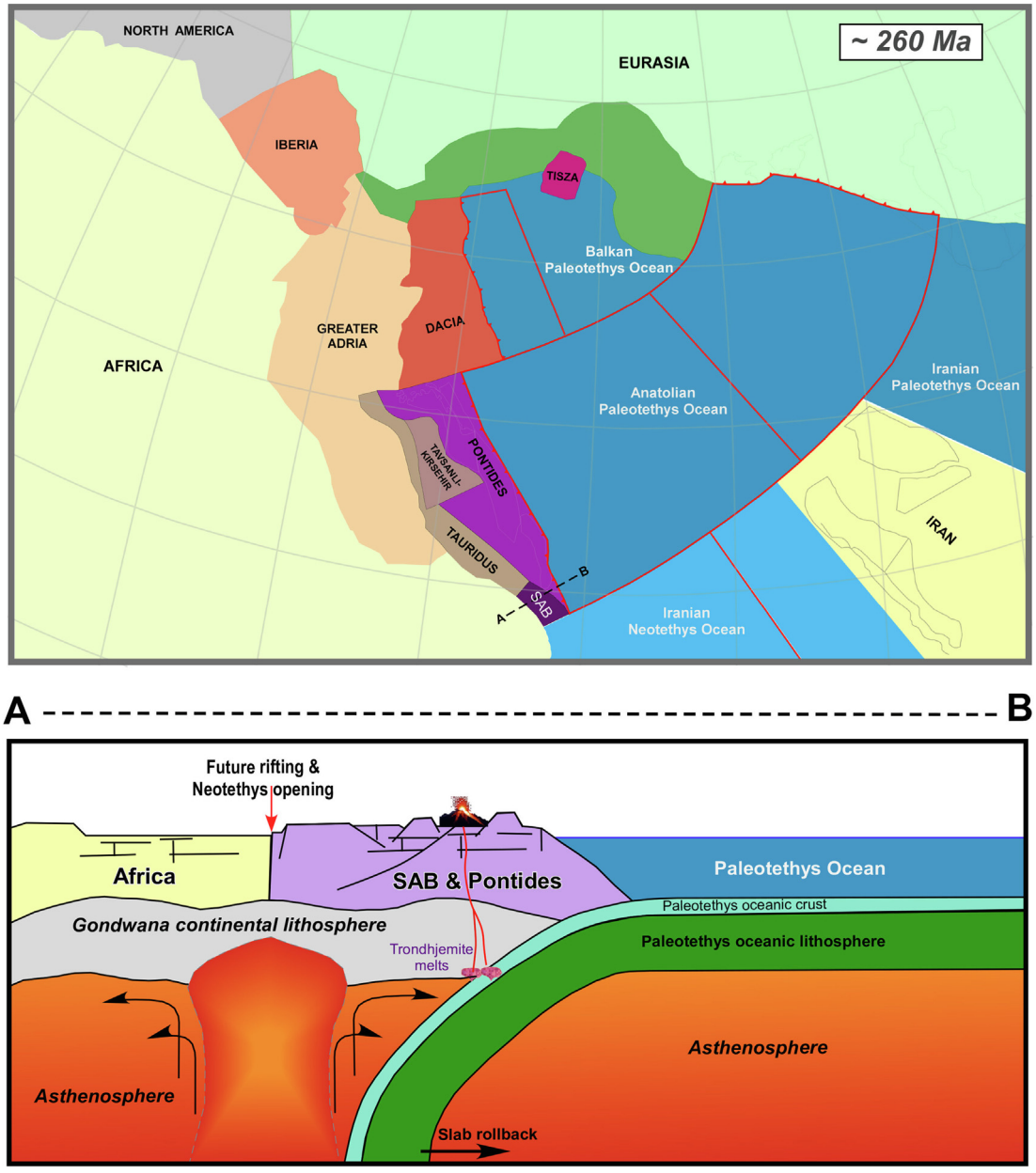

Fig. 15. Tectonic reconstruction of the SAB in the Tethyan realm during the Permian (260 Ma; map modified after van Hinsbergen et al., 2020).

6.2.2. Middle Triassic sills at Arpi, Darasham, and Khor Virap

Mafic OIB-type intrusions were emplaced into the Late Devonian sedimentary cover of the SAB at Arpi (Fig. 1) at 246.0 ± 3.3 Ma. Similar intrusions are also present in the Late Devonian sediments in south Nakhichevan (Darasham section; K-Ar age of 239 ± 7 Ma; Khanzatian, 1992). The major element compositions of the Arpi and Darasham basalts are virtually identical (Supplementary Fig. S3). Their OIB-type geochemistry indicates parental magmas derived from the asthenosphere, similar to late Palaeozoic rift-related basaltic magmatism of the northern Indian Gondwana margin and surrounding areas (e.g., Chauvet et al., 2008; Lapierre et al., 2004; Shellnutt et al., 2014; Wang et al., 2019; Zeng et al., 2019). Slightly later, at 233.7 ± 5.1 Ma, a mafic P-MORB-like sill also intruded the Late Devonian sedimentary cover of the SAB at Khor Virap (Fig. 1).

It is generally assumed that sills and dykes, similar to the ones reported here, represent the plumbing systems of ascending mantle-derived magmas (e.g., Coetzee and Kisters, 2017). The studied igneous rocks (section 3.2) likely represent parts of former feeder dykes or remnants of fissure eruption conduits. It is noteworthy that outcrops of these subvolcanic bodies abound only in a relatively small area (~1,500 km^2) of Upper Palaeozoic sequences of the SAB in Armenia and Nakhichevan, but that they probably signal an episode of magmatism at a much wider scale, since similar dyke and sill swarms are widespread in neighbouring Gondwana-derived units (e.g., Jones et al., 2001; Gaggero et al., 2012; Xu et al., 2016; Svensen et al., 2018; Wang et al., 2019). Particularly in Iran, a wide assortment of mafic subvolcanic intrusions in Upper Devonian and Lower Carboniferous sequences has been documented: in the Azerbaijan province (NW Iran; Alavi and Bolourchi, 1973), the Nain-Kerman region (Central Iran; Wendt et al., 2002; Hairapetian and Yazdi, 2003) and the Alborz Mountains (N-NE Iran; Ghavidel-Syooki, 1994, 1995; Mahmudy Gharaie, 2002; Ghavidel-Syooki and Owens, 2007). Radiometric age dates and geochemical details are generally lacking, but many have been linked to large-scale trap volcanism (Mahmudy Gharaie

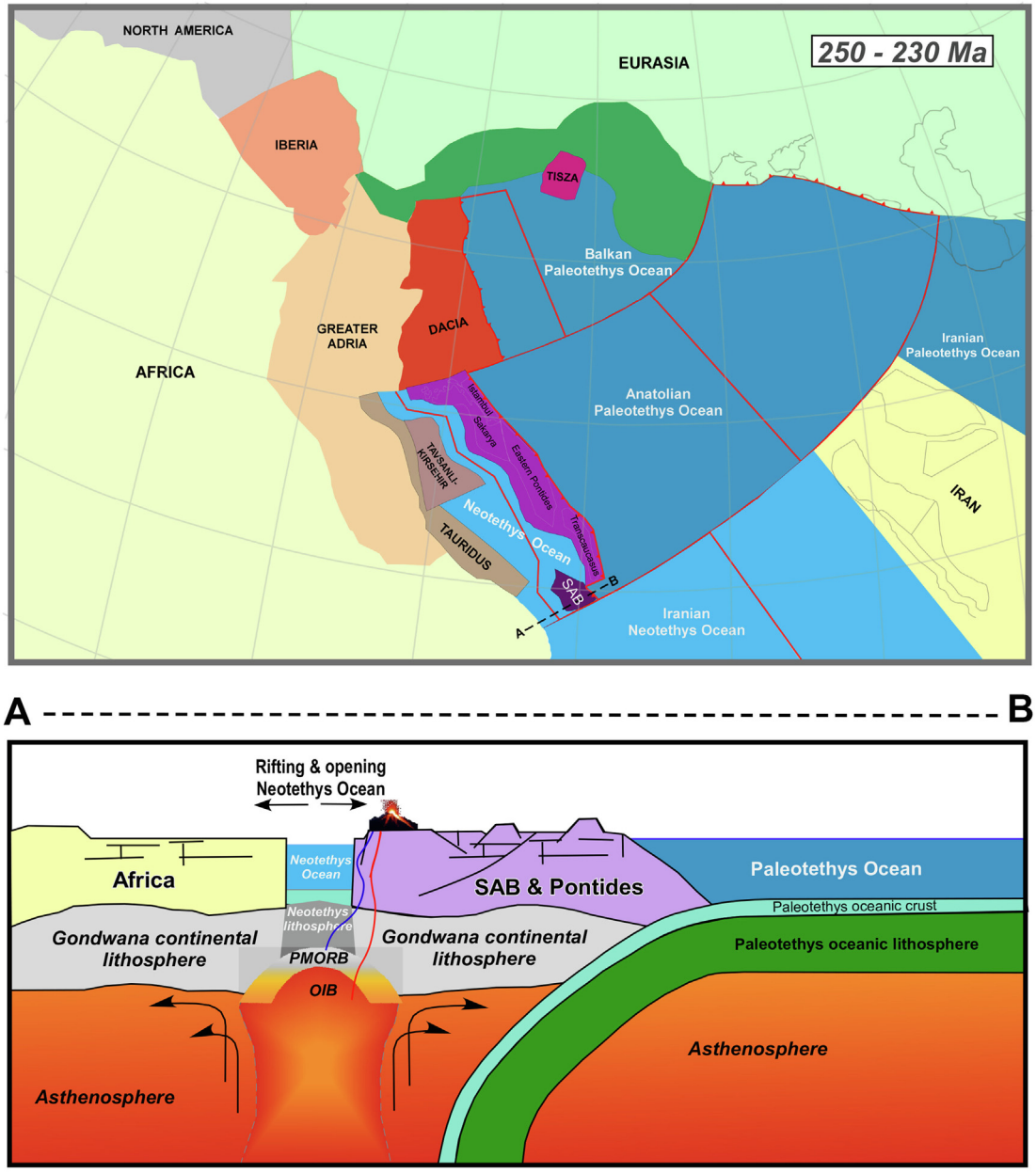

Fig. 16. Tectonic reconstruction of the SAB in the Tethyan realm during the Early-Middle Triassic (230–250 Ma; map modified after van Hinsbergen et al., 2020).

et al., 2004) and are thought to be considerably younger than the Upper Devonian country rocks (Wendt et al., 2002). Available data for one location confirm an intraplate (OIB-type) affinity (Mahmudy Gharaie, 2002).

The transition from OIB- to P-MORB-type magmatism within the short time interval of ~10 Ma is consistent with a change from a more enriched to a more depleted asthenospheric mantle source during melting at gradually shallower levels. Such associations of MORBs variably enriched by OIB-type components are typical for many *peri*-Mediterranean ophiolite complexes (e.g., Saccani and Photiades, 2005, and references therein), the Kermanshah ophiolite and Sistan suture zone in Iran (Saccani et al., 2010, 2013a), Oman ophiolites (Lapierre et al., 2004; Chauvet et al., 2011) and modern ocean basins (e.g., Le Roex et al., 1983, 1985; Haase and Devey, 1996). The generation of basaltic melts with OIB to MORB signatures is often an expression of asthenospheric upwelling and lithospheric extension that accompany initial continental rifting and subsequent (incipient) oceanic spreading (McKenzie and Bickle, 1988; Gorring et al., 2003; Saccani et al., 2013a).

The intrusions in the sedimentary cover of the SAB at Arpi, Darasham and Khor Virap (Fig. 1) between ~246 and 234 Ma thus suggest that the SAB experienced an episode of extension during latest Middle Triassic times. Together with the slightly earlier emplacement of arc-related granitoids in the metamorphic basement at ~262 Ma (closer to the active NE margin), this provides time constraints on rift initiation in the region. We infer that the asthenosphere-derived magmatic bodies record the incipient stage of breakup of the NE margin of Gondwana in the SAB region, and hence the opening of the Neotethys Ocean between the SAB and Africa in Middle Triassic times (Fig. 16).

The palaeomagnetic declinations of ARP-1,4 (~246 Ma) and KV-1 (~189 Ma) (Supplementary Data S1) plot between the values inferred for Africa and Eurasia (Fig. 14a). If we account for the

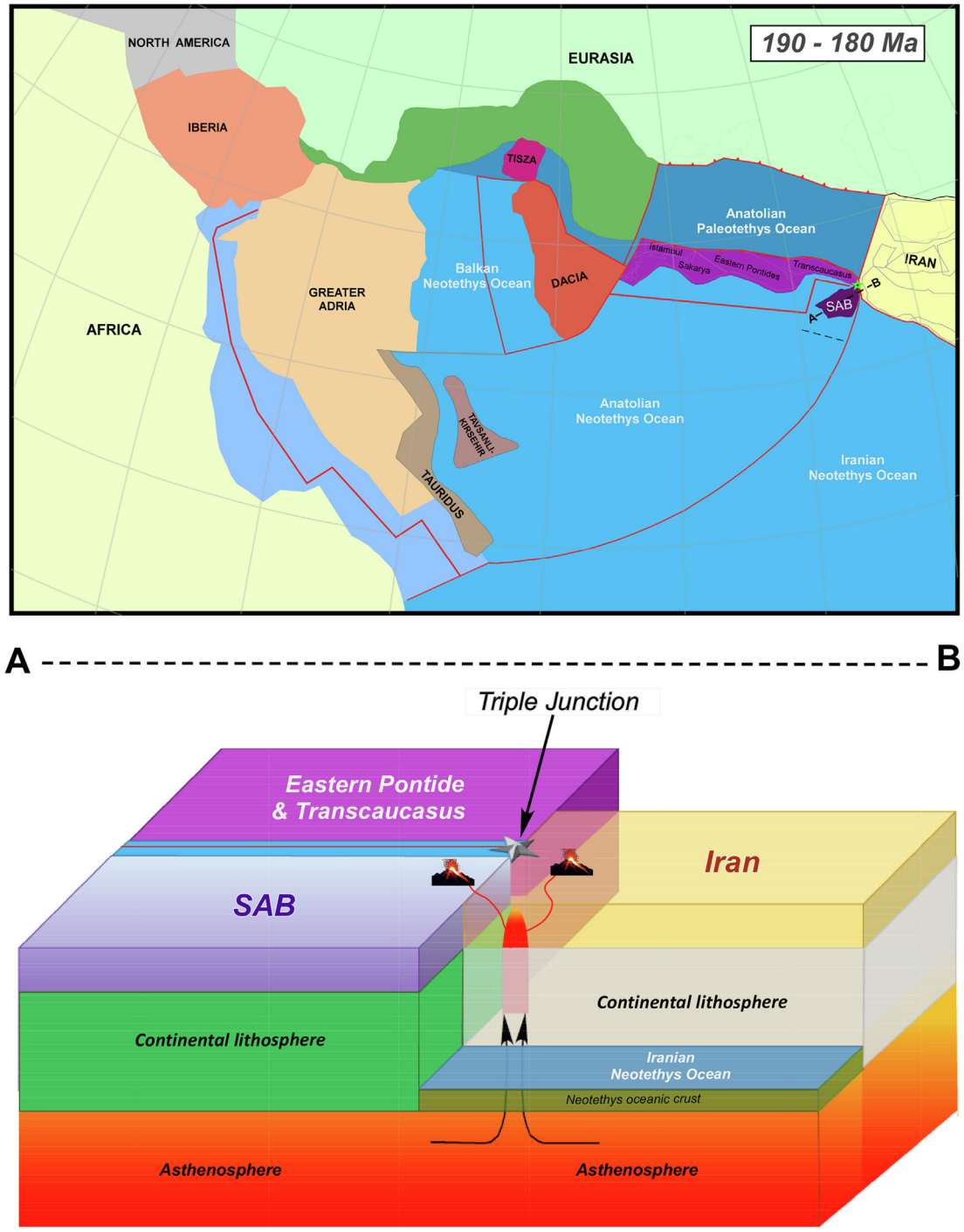

Fig. 17. Tectonic reconstruction of the SAB in the Tethyan realm during the Early Jurassic (180–190 Ma; map modified after van Hinsbergen et al., 2020).

assumed counterclockwise rotation of the SAB during its drift from the African to the Eurasian position, the declinations are more in agreement with Africa before 250 Ma, and more with Eurasia after 250 Ma (Fig. 14a). Accordingly, the results suggest that the rotation relative to Africa started before 250 Ma, and that the rotation relative to Eurasia was accomplished at 246 Ma (green and purple dots in Fig. 14). Additional support for this interpretation comes from the elongation of directional data, where declination deviations at 246 Ma might suggest rotational motion during that time and more latitudinal motions at 189 Ma led to inclination deviations (Fig. 14). Overall, the palaeomagnetic data are consistent with a rotational movement of the SAB from a position juxtaposed north of Africa and south of Eurasia (next to the Pontides and the Iranian blocks) between ~263 Ma and ~189 Ma, with most of the rotation having been completed before 240 Ma.

6.3. Mesozoic Tethyan realm: Evolution of the SAB

Lack of unequivocal geological evidence from the Armenian territory, owing to the extensive Cenozoic (volcano-)sedimentary cover, has hampered the reconstruction of the Mesozoic northward drift of the SAB in the Tethyan realm. In recent years, a significant effort has been made to reconstruct the tectonic evolution of the SAB from the Permian Gondwanan breakup to the Jurassic accre-

tion onto the Eurasian margin (Rolland et al., 2012) and the Miocene closure of the Neotethys by the Arabia-Eurasia collision (Okay et al., 2010; Cavazza et al., 2018). Most work has focused on the ophiolite complexes (Sevan-Akera, Vedi and Zangezur), thought to represent suture zones delimitating continental micro-blocks, and the metamorphic events preserved therein. The Jurassic–Cretaceous mafic intrusions in the Late Devonian sedimentary cover of the SAB at Khor Virap and Arpi (Fig. 1) provide more reliable, in-situ derived constraints on its Mesozoic evolution than the surrounding ophiolites, whose palaeo-positions with respect to the block are ambiguous.

6.3.1. Early Jurassic intrusions at Khor Virap

The Late Devonian sediments at Khor Virap also host two igneous sills consisting of intraplate OIB-type basalts dated at 188.5 ± 1.1 Ma. The only known, possibly contemporaneous, intracontinental igneous rocks in the SAB are Lower Jurassic basaltic rocks in the Negram–Julfa area (south Nahkichevan) and near the village of Aznaberd (Çalxanqala) in central Nakhichevan (Karyakin, 1989; Bazhenov et al., 1996), the locations of which are shown in Fig. 3a and 4. Their age was not radiometrically determined, but the work of Karyakin (1989) and geological mapping place the rocks unconformably between Middle-Upper Triassic and Middle Jurassic sediments. Although detailed geochemical data are lacking, these alkali basalts have an OIB-type "continental rifting" signature (Karyakin, 1989), similar to the Khor Virap OIB intrusions. All of these occurrences, from Khor Virap to Aznaberd to Negram, are positioned along a NW-SE-striking alignment (Fig. 1).

Based on their geochemical similarities, spatial association, and potential synchronicity, it is tempting to associate this Early Jurassic magmatism to lithospheric thinning and/or asthenospheric upwelling on the scale of the entire SAB, but this seems difficult to reconcile with existing geodynamic interpretations. Van Hinsbergen et al. (2020) used the palaeolatitude constraints of Bazhenov et al. (1996) and Meijers et al. (2015) to envisage the SAB as an isolated microcontinent during this period, left behind after an apparent Late Triassic ridge jump from south to north

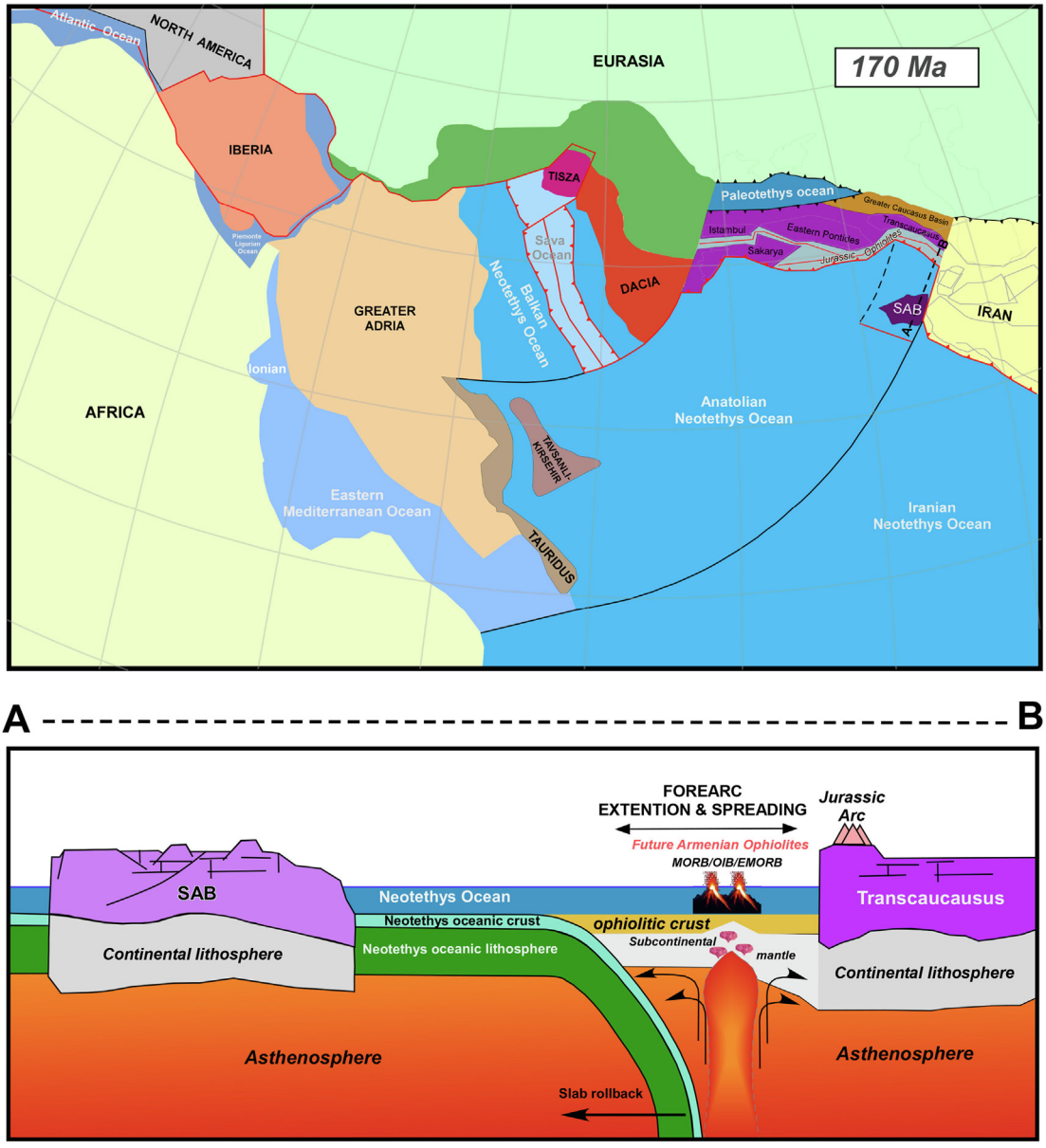

Fig. 18. Tectonic reconstruction of the SAB in the Tethyan realm during the Middle Jurassic (170 Ma; map modified after van Hinsbergen et al., 2020).

(Fig. 45 of van Hinsbergen et al., 2020), although constraints from the Triassic-Jurassic key interval are limited. Such a scenario would, however, not offer an obvious trigger for asthenospheric melting that the igneous rocks imply.

If we disregard the palaeolatitude of Bazhenov et al. (1996), in absence of a reliable age constraint, and consider the analytical uncertainty of our new position at 188.5 ± 1.1 Ma (Fig. 14; Supplementary Data S1), a scenario is conceivable in which the SAB continued its northward drift along with the Pontides (van Hinsbergen et al., 2020), and was already close to the Eurasian margin during the Early Jurassic. This is in line with the absence of evidence for any 'stranding' of the SAB in the Neotethys behind the eastern Pontides, although tighter palaeomagnetic testing is obviously needed. In this scenario the SAB met the Iranian block at about 190 Ma (Fig. 17), remarkably coinciding with the age of the studied intraplate magmatism. We propose this scenario as an update of the 'isolated island' interpretation of van Hinsbergen et al. (2020), as it provides a plausible explanation for the magmatic event. The rise of intraplate basalts may be facilitated by the presence of a plate boundary, as in the case of the Anatolian–African–Arabian plate junction in southeastern Turkey (Nikogosian et al., 2018). It is therefore conceivable that a similar setting along the triple junction between the SAB, Pontides-Transcaucasus and Iran triggered mantle melting and emplacement of the intraplate basalts of Khor Virap, Aznaberd, and Negram (Fig. 17).

6.3.2. Generation of the Armenian ophiolites

Current interpretations of the SAB are based chiefly on ophiolitic remnants in Armenia and the assumed Mesozoic palaeoposition of Bazhenov et al. (1996). Many authors have adopted the view that the drift history of the SAB was identical to that of the Taurides (Okay and Tüysüz, 1999; Barrier and Vrielynck, 2008; Rolland et al., 2012; Meijers et al., 2015). An alternative reconstruction (van Hinsbergen et al., 2020) proposes that the

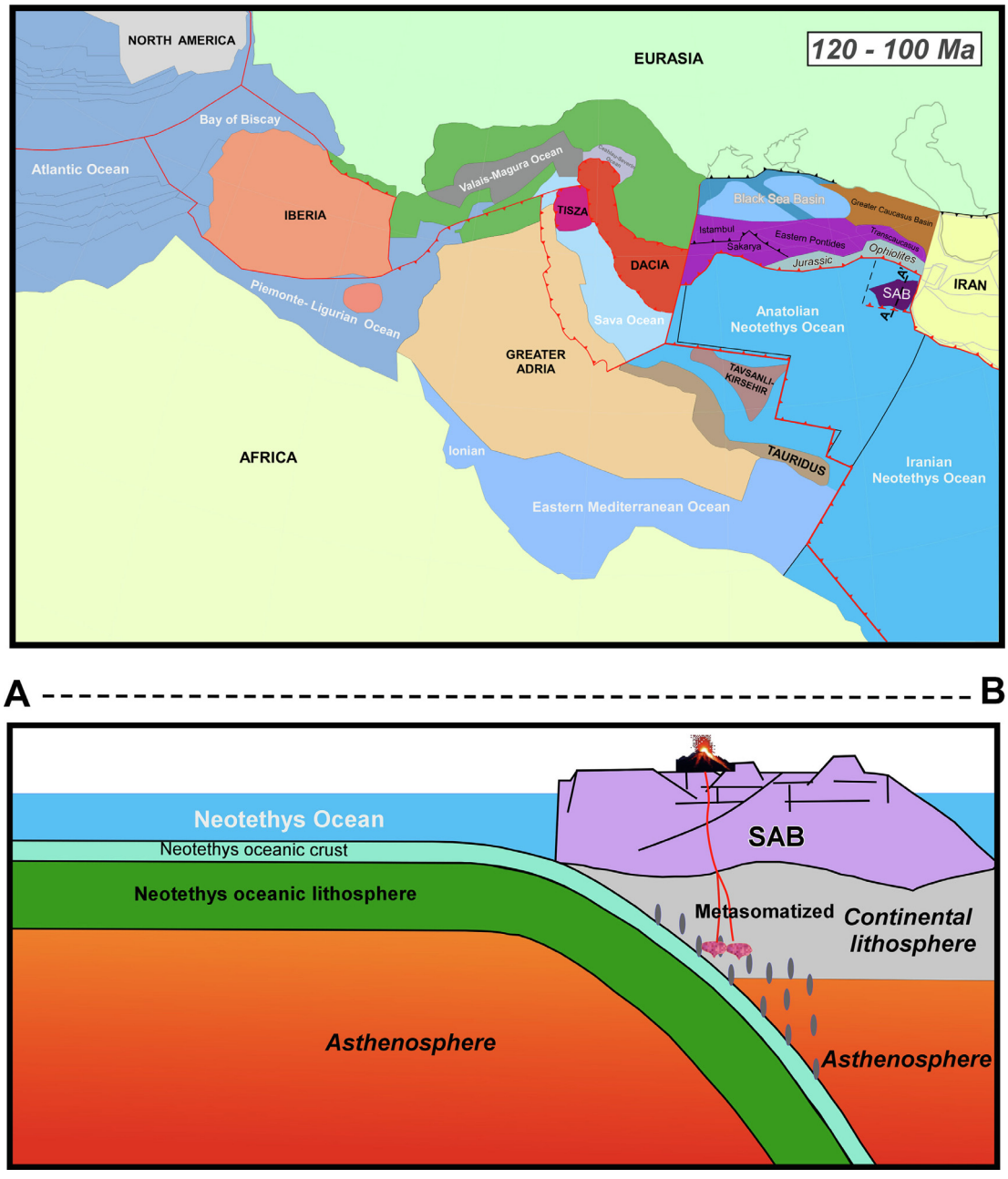

Fig. 19. Tectonic reconstruction of the SAB in the Tethyan realm during the Early Cretaceous (100–120 Ma; map modified after van Hinsbergen et al., 2020).

Taurides drifted away from Gondwana much later (<200 Ma) than the SAB (~245 Ma), and that this ~50 Myr 'lag' persisted throughout the Mesozoic until the collision with Eurasia. According to this scenario all of the Armenian ophiolites formed in a forearc setting close to the Eurasian margin (van Hinsbergen et al., 2020), which is consistent with our suggested Middle Jurassic position of the SAB against the western boundary of the Iranian continent, a few hundred kilometres south of the Transcaucausus (Fig. 18). It explains the occurrence of MORB, OIB and E-MORB-type rocks (e.g., Rolland et al., 2020), as well as rare boninites in the SAB (Magakyan et al., 1993). Extension of the forearc region and eventual slab rollback (Fig. 18b) could have halted the SAB drift and initiate NE-directed subduction on the southern margin of the SAB.

6.3.3. Early Cretaceous (Albian) intrusions at Arpi and Darasham

In addition to the Middle Triassic alkaline intrusions, the Late Devonian sedimentary cover in the Arpi area also hosts an andesitic neck dated at 116.7 ± 1.5 Ma. They also have a clear parallel in the Darasham section in south Nakhichevan (Fig. 4), where an andesitic dyke (104.0 ± 2.2 Ma) and amphibole-bearing basaltic dyke (126.0 ± 2.1 Ma) have been found (Khanzatian, 1992). Their trace-element contents showing a subduction-related imprint are common geochemical signatures. Moreover, the Sr-Nd isotope compositions (Fig. 10e) of the Arpi andesite suggest source contamination by subducted crustal components. When the occurrence of slightly older (140–155 Ma) arc-type granodiorite intrusions in the SAB (Hässig et al., 2015; Galoyan et al., 2018, 2020) are also considered, this coexistence of subduction-associated magmatism in Armenia and Nakhichevan likely points to an active subduction system, at least during this (late) Early Cretaceous period (Fig. 19).

The arc-type granodiorite intrusions into the SAB basement at 140–155 Ma that have previously been explained by SW-dipping subduction (Hässig et al., 2015; Galoyan et al., 2018, 2020) in our interpretation are best explained by a NE-directed subduction zone at the southern margin of the SAB in Late Jurassic to Early Cretaceous times (Fig. 19). This subduction possibly initiated as a result of forearc spreading at the Eurasian margin, halting the SAB and accommodating continued Africa-Eurasia convergence to its south. The Early Cretaceous andesitic and basaltic sills in the Darasham section in south Nakhichevan (Khanzatian, 1992), and the Arpi andesitic intrusion of ~117 Ma possibly represent a continuation of this subduction-related igneous activity. This NE-directed subduction system obviates the need for one or more separate, coexisting active margins to explain the presence of the intrusive rocks (e.g., Hässig et al., 2015; Rolland, 2017; Galoyan et al., 2020), which seems unlikely given the convergence rate required to sustain multiple subduction zones.

7. Conclusions

We report new geochronological, geochemical, and palaeomagnetic data on magmatic intrusions into the Late Devonian sedimentary cover, and metamorphic rocks that constitute part of the basement of the South Armenian Block. These data are used to place new constraints on the origin and geodynamic history of the SAB in the context of Permian–Triassic breakup of the NE Gondwanan margin, the opening of the Neotethys Ocean, and the Mesozoic kinematic history of the SAB. Our conclusions can be summarised as follows:

1. The characteristic Neoproterozoic–Palaeozoic U-Pb age peaks of detrital zircons derived from the Armenian metamorphic basement firmly establish a Gondwanan origin of the SAB.
2. The geochemistry of trondhjemite ("plagiogranite") intrusions into the Armenian metamorphic basement at ~263 Ma demonstrates their adakite/TTG affinity and reflects magma genesis in an active continental margin, consistent with a SW-dipping subduction zone active at the NE Gondwanan margin (Pontides and SAB) during the Middle–Late Permian.
3. Mafic alkaline OIB-like sills in the Late Devonian sedimentary cover in the Arpi (south central Armenia) and Darasham (south Nakhichevan) areas, dated at ~246 Ma, are products of asthenospheric melting beneath the SAB. A mafic P-MORB-like intrusion at Khor Virap, dated at ~234 Ma, reflects melt derivation from a more depleted, shallower mantle source. This set of intrusions is typical of initial continental rifting and early-stage oceanic spreading and suggests a phase of extensional tectonics in the SAB during the Middle Triassic. We infer that this activity marks the incipient breakup of the NE Gondwanan margin and subsequent opening of the Neotethys Ocean in the area.
4. Mafic alkaline OIB-type sills within the Late Devonian sedimentary cover at Khor Virap (south central Armenia), dated at ~189 Ma, testify to another episode of magma production in the shallow asthenospheric mantle beneath the SAB. In our interpretation the SAB continued its northwards drift alongside the eastern Pontides and reached the Iranian block at about 190 Ma. The intraplate magmatism is likely associated with the triple junction between the SAB, Pontides-Transcaucasus and Iran.
5. Andesitic dykes in the Late Devonian sedimentary cover in the Arpi (~117 Ma) and Darasham (104–126 Ma) areas exhibit a "subduction-related" geochemical signature, consistent with melt derivation from subduction-modified lithospheric mantle, which also applies to other sporadic occurrences of Late Jurassic to Early Cretaceous igneous products in the SAB. This subduction-related magmatism can be explained by a NE-directed subduction system at the southern margin of the SAB, driven by forearc spreading in the Eurasian margin, which led to cessation of the SAB drift and accommodated compression south of the SAB in Late Jurassic–Early Cretaceous times.

Declaration of Competing Interest

The authors declare that they have no known competing financial interests or personal relationships that could have appeared to influence the work reported in this paper.

Acknowledgements

We gratefully acknowledge Dr. Vilen Aghamalyan for his decades-long study of the Tsakhkunyats metamorphic basement and great contribution in revealing its complex geology, as well as for help in selecting representative samples. We thank Pieter Vroon and Helen de Waard for their help with XRF and ICP-MS analyses, respectively, and Roel van Elsas for sample preparation. We thank Dr. Iain Neill and an anonymous reviewer for their constructive comments, and Dr. Andrea Festa for editorial handling. This research was partially supported by The Netherlands Research Centre for Integrated Solid Earth Science (ISES) through grant 6.2.12. IKN, AJJBG and JMK acknowledge financial support from the European Research Council (ERC) under the European Union's Horizon 2020 research and innovation programme (grant agreement n° 759563). The Armenian team was supported by the State base funding of the Institute of Geological Sciences of the Armenian Academy of Sciences. The data used are listed in the supplementary material, tables and references.

Appendix A. Supplementary data

Supplementary data to this article can be found online at https://doi.org/10.1016/j.gr.2023.03.023.

References

Abbo, A., Avigad, D., Gerdes, A., Güngör, T., 2015. Cadomian basement and Paleozoic to Triassic siliciclastics of the Taurides (Karacahisar dome, south-central Turkey): Paleogeographic constraints from U-Pb–Hf in zircons. Lithos 227, 122–139. https://doi.org/10.1016/J.LITHOS.2015.03.023.

Adamia, S.A., Chkhotua, T., Kekelia, M., Lordkipanidze, M., Shavishvili, I., Zakariadze, G., 1981. Tectonics of the Caucasus and adjoining regions: Implications for the evolution of the Tethys ocean. J. Struct. Geol. 3, 437–447. https://doi.org/10.1016/0191-8141(81)90043-2.

Adamia, S.A., Chkhotua, T.G., Gavtadze, T.T., Lebanidze, Z.A., Lursmanashvili, N.D., Sadradze, N.G., Zakaraia, D.P., Zakariadze, G.S., 2017. Tectonic setting of Georgia-Eastern Black Sea: A review. Geol. Soc. London. Spec. Publ. 428, 11–40. https://doi.org/10.1144/SP428.6.

Adamia, S., Bergougnan, H., Fourquin, C., Haghipour, A., Lordkipanidze, M., Ozgül, N., Ricou, L., Zakariadze, G., 1980. The Alpine Middle East between the Aegean and the Oman traverses, in: 26th International Geological Congress Paris C. pp. 122–136.

Adamia, S., Zakariadze, G., Chkhotua, T., Sadradze, N., Tsereteli, N., Chabukiani, A., Gventsadze, A., 2011. Geology of the Caucasus: A review. Turkish J. Earth Sci. 20, 489–544.

Agard, P., Omrani, J., Jolivet, L., Whitechurch, H., Vrielynck, B., Spakman, W., Monié, P., Meyer, B., Wortel, R., 2011. Zagros orogeny: A subduction-dominated process. Geol. Mag. 148, 692–725. https://doi.org/10.1017/S001675681100046X.

Aghamalyan, V.A., 1983. Pre-Cambrian stratigraphy of the Armenian SSR (in Russian). Proc. NAS R.A. Earth Sci. 4, 26–39.

Aghamalyan, V.A., 1998. The basement crystalline of Armenia. National Academy of Sciences of Armenia (Yerevan). in Russian.

Aghamalyan, V.A., Mayringer, F., Lorsabyan, T., Israelyan, A., 2011. Geochemical features of pre-Cambrian amphibolites of the Armenian crystalline massif as a fragment of metamorphosed basalts of the pan-African oceanic crust. Proc. Natl. Acad. Sci. Armen. Earth Sci. 64, 15–23.

Aghamalyan, V.A., 1978. The old metamorphic complexes of the territory of Armenian SSR and their tectonic disposition, in: Proceedings of Reports of the Second Regional Petrographic Symposium on Caucasus, Crimea and Carpathians. Tbilisi. p. 115.

Aghamalyan, V.A., 2004. The Lesser Caucasus earth crust formation and evolution in the collision zone of Paleo-Tethys, in: Chatzipetros, A.A., Pavlides, S.B. (Eds.), Proceedings of the 5th International Symposium on Eastern Mediterranean Geology. Thessaloniki, Greece, pp. 17–20.

Agranier, A., Blichert-Toft, J., Graham, D., Debaille, V., Schiano, P., Albarede, F., 2005. The spectra of isotopic heterogeneities along the mid-Atlantic Ridge. Earth Planet. Sci. Lett. 238, 96–109. https://doi.org/10.1016/j.epsl.2005.07.011.

Alavi, M., 1991. Sedimentary and structural characteristics of the Paleo-Tethys remnants in northeastern Iran. Geol. Soc. Am. Bull. 103, 983–992. https://doi.org/10.1130/0016-7606(1991)103<0983:SASCOT>2.3.CO;2.

Alavi, M., Bolourchi, H., 1973. Geology of the Makou area. Surv. Iran, Rep. No. Al, Geol.

Alizadeh, A.A., 2008. Geological map of Azerbaijan Republic, 1:500,000.

Anczkiewicz, R., Oberli, F., Burg, J.P., Villa, I.M., Günther, D., Meier, M., 2001. Timing of normal faulting along the Indus Suture in Pakistan Himalaya and a case of major 231Pa/235U initial disequilibrium in zircon. Earth Planet. Sci. Lett. 191, 101–114. https://doi.org/10.1016/S0012-821X(01)00406-X.

Arakelyan, R.A., 1957. Stratigraphy of metamorphic complex of Armenia (in Russian). Proc. NAS R.A Earth Sci. 10, 3–16.

Arakelyan, R.A., 1952. Paleozoic stratigraphy of southwest Armenia and adjacent regions of the Nakhichevan Autonomous Republic (in Russian). Yerevan AN Arm. SSR.

Arakelyan, R.A., 1964. The Paleozoic–Mesozoic. The Geology of the Armenian SSR: Stratigraphy. Publ. House Acad. Sci. Armen. SSR 21–63.

Aslanyan, A.T., 1958. Regional geology of Armenia. Izv, Haypethrat, Yerevan, p. 430.

Avagyan, A.V., Sahakyan, L.G., Sosson, M., Vardanyan, S.S., Martirosyan, M.P., 2015. Tectonics of the south-east Ararat depression [in Armenian]. Proc. NAS R.A. Earth Sci. 68, 47–66.

Avagyan, A., Sosson, M., Sahakyan, L., Sheremet, Y., Vardanyan, S., Martirosyan, M., Muller, C., 2018. Tectonic evolution of the northern margin of the Cenozoic Ararat Basin, Lesser Caucasus. Armenia. J. Pet. Geol. 41, 495–511. https://doi.org/10.1111/jpg.12718.

Aysal, N., Öngen, S., Peytcheva, I., Keskin, M., 2012. Origin and evolution of the Havran Unit, Western Sakarya basement (NW Turkey): New LA-ICP-MS U-Pb dating of the metasedimentary-metagranitic rocks and possible affiliation to Avalonian microcontinent. Geodin. Acta 25, 226–247. https://doi.org/10.1080/09853111.2014.882536.

Azizbekov, S.A., 1962. Geology of lead-zinc deposits in the Caucasus and patterns of their distribution (in Russian). Gosgeoltechizdat.

Azizi, H., Chung, S.-L., Tanaka, T., Asahara, Y., 2011. Isotopic dating of the Khoy metamorphic complex (KMC), northwestern Iran: A significant revision of the formation age and magma source. Precambrian Res. 185, 87–94. https://doi.org/10.1016/j.precamres.2010.12.004.

Balaghi Einalou, M., Sadeghian, M., Zhai, M., Ghasemi, H., Mohajjel, M., 2014. Zircon U-Pb ages, Hf isotopes and geochemistry of the schists, gneisses and granites in Delbar Metamorphic-Igneous Complex, SE of Shahrood (Iran): Implications for Neoproterozoic geodynamic evolutions of Central Iran. J. Asian Earth Sci. 92, 92–124. https://doi.org/10.1016/j.jseaes.2014.06.011.

Ballard, J.R., Palin, M.J., Campbell, I.H., 2002. Relative oxidation states of magmas inferred from Ce(IV)/Ce(III) in zircon: Application to porphyry copper deposits of northern Chile. Contrib. to Mineral. Petrol. 144, 347–364. https://doi.org/10.1007/s00410-002-0402-5.

Barrier, E., Vrielynck, B., 2008. Paleotectonic maps of the Middle East – Atlas of 14 maps, in: Middle East Basin Evolution Programme.

Bazhenov, M.L., Burtman, V.S., Levashova, N.L., 1996. Lower and Middle Jurassic paleomagnetic results from the south Lesser Caucasus and the evolution of the Mesozoic Tethys ocean. Earth Planet. Sci. Lett. 141, 79–89. https://doi.org/10.1016/0012-821X(96)00056-8.

Belousova, E.A., Griffin, W.L., O'Reilly, S.Y., 2006. Zircon crystal morphology, trace element signatures and Hf isotope composition as a tool for petrogenetic modelling: examples from Eastern Australian granitoids. J. Petrol. 47, 329–353. https://doi.org/10.1093/petrology/egi077.

Belov, A.A., Sokolov, S.D., 1973. Relicts of Mesozoic oceanic crust among the crystalline complexes of the Miskhana massif of Armenia (in Russian). Sov. Geol. 8, 26–41.

Berberian, M., King, G.C.P., 1981. Towards a paleogeography and tectonic evolution of Iran. Can. J. Earth Sci. 18, 210–265. https://doi.org/10.1139/e81-019.

Bouvier, A., Vervoort, J.D., Patchett, P.J., 2008. The Lu-Hf and Sm-Nd isotopic composition of CHUR: Constraints from unequilibrated chondrites and implications for the bulk composition of terrestrial planets. Earth Planet. Sci. Lett. 273, 48–57. https://doi.org/10.1016/j.epsl.2008.06.010.

Brunet, M.-F., Korotaev, M.V., Ershov, A.V., Nikishin, A.M., 2003. The South Caspian Basin: A review of its evolution from subsidence modelling. Sediment. Geol. 156, 119–148. https://doi.org/10.1016/S0037-0738(02)00285-3.

Candan, O., Akal, C., Koralay, O.E., Okay, A.I., Oberhänsli, R., Prelević, D., Mertz-Kraus, R., 2016. Carboniferous granites on the northern margin of Gondwana, Anatolide-Tauride Block, Turkey – Evidence for southward subduction of Paleotethys. Tectonophysics 683, 349–366. https://doi.org/10.1016/J.TECTO.2016.06.030.

Cavazza, W., Cattò, S., Zattin, M., Okay, A.I., Reiners, P., 2018. Thermochronology of the Miocene Arabia-Eurasia collision zone of southeastern Turkey. Geosphere 14, 2277–2293. https://doi.org/10.1130/GES01637.1.

Chauvet, F., Lapierre, H., Bosch, D., Guillot, S., Mascle, G., Vannay, J.C., Cotten, J., Brunet, P., Keller, F., 2008. Geochemistry of the Panjal Traps basalts (NW Himalaya): Records of the Pangea Permian break-up. Bull. la Soc. Geol. Fr. 179, 383–395. https://doi.org/10.2113/gssgfbull.179.4.383.

Chauvet, F., Lapierre, H., Maury, R.C., Bosch, D., Basile, C., Cotten, J., Brunet, P., Campillo, S., 2011. Triassic alkaline magmatism of the Hawasina Nappes: Post-breakup melting of the Oman lithospheric mantle modified by the Permian Neotethyan Plume. Lithos 122, 122–136. https://doi.org/10.1016/j.lithos.2010.12.006.

Chiu, H.-Y., Zarrinkoub, M.H., Melkonyan, R., Pang, K.-N., Lee, H.-Y., Wang, K.-L., Mohammadi, S.S., Khatib, M.M., 2017. Zircon Hf isotopic constraints on magmatic and tectonic evolution in Iran: Implications for crustal growth in the Tethyan orogenic belt. J. Asian Earth Sci. 145, 652–669. https://doi.org/10.1016/J.JSEAES.2017.06.011.

Coetzee, A., Kisters, A.F.M., 2017. Dyke-sill relationships in Karoo dolerites as indicators of propagation and emplacement processes of mafic magmas in the shallow crust. J. Struct. Geol. 97, 172–188. https://doi.org/10.1016/j.jsg.2017.03.002.

Cox, K.G., Bell, J.D., Pankhurst, R.J., 1979. The interpretation of igneous rocks. Springer, Netherlands, Dordrecht. https://doi.org/10.1007/978-94-017-3373-1.

Danelian, T., Robertson, A.H.F., Collins, A.S., Poisson, A., 2006. Biochronology of Jurassic and Early Cretaceous radiolarites from the Lycian Mélange (SW Turkey) and implications for the evolution of the Northern Neotethyan ocean. Geol. Soc. London. Spec. Publ. 260, 229–236. https://doi.org/10.1144/GSL.SP.2006.260.01.10.

Danelian, T., Asatryan, G., Sahakyan, L., Galoyan, G., Sosson, M., Avagyan, A., 2010. New and revised radiolarian biochronology for the sedimentary cover of ophiolites in the Lesser Caucasus (Armenia). Geol. Soc. London. Spec. Publ. 340, 383–391. https://doi.org/10.1144/SP340.16.

Danelian, T., Asatryan, G., Galoyan, G., Sahakyan, L., Stepanyan, J., 2016. Late Jurassic-Early Cretaceous radiolarian age constraints from the sedimentary cover of the Amasia ophiolite (NW Armenia), at the junction between the Izmir–Ankara–Erzinçan and Sevan-Hakari suture zones. Int. J. Earth Sci. 105, 67–80. https://doi.org/10.1007/s00531-015-1228-5.

Davoudzadeh, M., Schmidt, K., 1981. Contribution to the paleogeography and stratigraphy of the Upper Triassic to Middle Jurassic of Iran. Neues Jahrb. Geol. Palaontol. Abh. 162, 137–163.

De Laeter, J.R., Böhlke, J.K., De Bièvre, P., Hidaka, H., Peiser, H.S., Rosman, K.J.R., Taylor, P.D.P., 2003. Atomic weights of the elements. Review 2000 (IUPAC Technical Report). Pure Appl. Chem. 75, 683–800. https://doi.org/10.1351/pac200375060683.

Defant, M.J., Drummond, M.S., 1990. Derivation of some modern arc magmas by melting of young subducted lithosphere. Nature 347, 662–665. https://doi.org/10.1038/347662a0.

Dilek, Y., Furnes, H., 2019. Tethyan ophiolites and Tethyan seaways. J. Geol. Soc. London. jgs2019-129. Doi: 10.1144/jgs2019-129.
Dokuz, A., Aydınçakır, E., Kandemir, R., Karslı, O., Siebel, W., Derman, A.S., Turan, M., 2017. Late Jurassic magmatism and stratigraphy in the Eastern Sakarya Zone, Turkey: Evidence for the slab breakoff of Paleotethyan oceanic lithosphere. J. Geol. 125, 1–31.
Eggins, S.M., Woodhead, J.D., Kinsley, L.P.J., Mortimer, G.E., Sylvester, P., McCulloch, M.T., Hergt, J.M., Handler, M.R., 1997. A simple method for the precise determination of ≥ 40 trace elements in geological samples by ICPMS using enriched isotope internal standardisation. Chem. Geol. 134, 311–326. https://doi.org/10.1016/S0009-2541(96)00100-3.
Eyuboglu, Y., Santosh, M., Bektas, O., Chung, S.-L., 2011. Late Triassic subduction-related ultramafic–mafic magmatism in the Amasya region (eastern Pontides, N. Turkey): Implications for the ophiolite conundrum in Eastern Mediterranean. J. Asian Earth Sci. 42, 234–257. https://doi.org/10.1016/j.jseaes.2011.01.007.
Fan, Y., Xiao, Q., Li, T., Cheng, Y., Li, Y., Guo, L., Luo, P., 2022. Geochronology, geochemistry, Sr–Nd–Hf isotope composition of the late Permian adakite in West Ujimqin, Inner Mongolia: petrogenesis and tectonic implications. Can. J. Earth Sci. 59, 46–58. https://doi.org/10.1139/cjes-2019-0002.
Fazlnia, A., Schenk, V., van der Straaten, F., Mirmohammadi, M., 2009. Petrology, geochemistry, and geochronology of trondhjemites from the Qori Complex, Neyriz. Iran. Lithos 112, 413–433. https://doi.org/10.1016/J.LITHOS.2009.03.047.
Fergusson, C.L., Nutman, A.P., Mohajjel, M., Bennett, V.C., 2016. The Sanandaj-Sirjan Zone in the Neo-Tethyan suture, western Iran: Zircon U-Pb evidence of late Palaeozoic rifting of northern Gondwana and mid-Jurassic orogenesis. Gondwana Res. 40, 43–57. https://doi.org/10.1016/J.GR.2016.08.006.
Font, L., van der Peijl, G., van Wetten, I., Vroon, P., van der Wagt, B., Davies, G., 2012. Strontium and lead isotope ratios in human hair: investigating a potential tool for determining recent human geographical movements. J. Anal. At. Spectrom. 27, 719. https://doi.org/10.1039/c2ja10361c.
Gaggero, L., Oggiano, G., Funedda, A., Buzzi, L., 2012. Rifting and arc-related early Paleozoic volcanism along the north Gondwana margin: geochemical and geological evidence from Sardinia (Italy). J. Geol. 120, 273–292. https://doi.org/10.1086/664776.
Galoyan, G.L., Melkonyan, R.L., Atayan, L.S., Chung, S.-L., Khorenyan, R.H., Lee, Y.-H., Amiraghyan, S.V., 2018. On the petrology and geochemistry of Jurassic magmatics of the Somkheti segment of Somkheto-Karabagh tectonic zone (northern Armenia). Proc. Natl. Acad. Sci. Armen. Earth Sci. 71, 3–27.
Galoyan, G.L., Chung, S.-L., Melkonyan, R.L., Lee, Y.-H., Atayan, L.S., Ghukasyan, R.K., Khorenyan, R.H., Grigoryan, A.G., Sahakyan, S.S., Avagyan, N.A., 2020. Late Neoproterozoic-Early Cambrian, Late Paleozoic and Late Jurassic granitoid magmatism on the northern active margin of Gondwana, Tsaghkunyats anticlinorium of Lesser Caucasus (central-northern Armenia). Proc. NAS RA, Earth Sci. 73, 16–43.
Galoyan, G., Rolland, Y., Sosson, M., Corsini, M., Melkonyan, R., 2007. Evidence for superposed MORB, oceanic plateau and volcanic arc series in the Lesser Caucasus (Stepanavan, Armenia). Comptes Rendus Geosci. 339, 482–492. https://doi.org/10.1016/j.crte.2007.06.002.
Galoyan, G., Rolland, Y., Sosson, M., Corsini, M., Billo, S., Verati, C., Melkonyan, R., 2009. Geology, geochemistry and 40Ar/39Ar dating of Sevan ophiolites (Lesser Caucasus, Armenia): Evidence for Jurassic back-arc opening and hot spot event between the South Armenian Block and Eurasia. J. Asian Earth Sci. 34, 135–153. https://doi.org/10.1016/j.jseaes.2008.04.002.
Gealey, W.K., 1988. Plate tectonic evolution of the Mediterranean-Middle East region. Tectonophysics 155, 285–306. https://doi.org/10.1016/0040-1951(88)90270-3.
Gessner, K., Ring, U., Passchier, C.W., Güngör, T., 2001. How to resist subduction: Evidence for large-scale out-of-sequence thrusting during Eocene collision in western Turkey. J. Geol. Soc. London. 158, 769–784. https://doi.org/10.1144/jgs.158.5.769.
Ghaderi, A., Taherpour Khalil Abad, M., Ashouri, A.R., Korn, D., 2016. Permian Calcareous algae from the Khachik Formation at the Ali Bashi Mountains, NW of Iran. Arab. J. Geosci. 9, 699. https://doi.org/10.1007/s12517-016-2737-7.
Ghavidel-Syooki, M., 1995. Palynostratigraphy and palaeogeography of a Palaeozoic sequence in the Hassanakdar area, Central Alborz Range, northern Iran. Rev. Palaeobot. Palynol. 86, 91–109. https://doi.org/10.1016/0034-6667(94)00100-X.
Ghavidel-Syooki, M., Owens, B., 2007. Palynostratigraphy and palaeogeography of the Padeha, Khoshyeilagh, and Mobarak formations in the eastern Alborz Range (Kopet-Dagh region), northeastern Iran. Rev. Micropaléontologie 50, 129–144. https://doi.org/10.1016/J.REVMIC.2007.01.004.
Ghavidel-Syooki, M., 1994. Biostratigraphy and paleo-biogeography of some Paleozoic rocks at Zagross and Alborz mountains, in: Hushmand-zadeh, A. (Ed.), Treatise on the Geology of Iran. Tehran, Iran, p. 168.
Ginter, M., Hairapetian, V., Grigoryan, A., 2011. Chondrichthyan microfossils from the Famennian and Tournaisian of Armenia. Acta Geol. Pol. 61, 153–173.
Gorring, M., Singer, B., Gowers, J., Kay, S.M., 2003. Plio-Pleistocene basalts from the Meseta del Lago Buenos Aires, Argentina: evidence for asthenosphere–lithosphere interactions during slab window magmatism. Chem. Geol. 193, 215–235. https://doi.org/10.1016/S0009-2541(02)00249-8.
Grachev, A.F., Karyakin, Y.V., 1983. Formation affiliation of volcanic series: The example of the Early Jurassic volcanic rocks of the Nakhichevan ASSR (in Russian). Abstracts of IV Regional Petrographic Meeting on the Caucasus, Crim and Carpathians., 18–20
Grigoryan, A., 1990. The conodonts of the Permian-Triassic boundary in Armenia. Lomonosov Moscow State University. in Russian.
Grimes, C.B., John, B.E., Kelemen, P.B., Mazdab, F.K., Wooden, J.L., Cheadle, M.J., Hanghøj, K., Schwartz, J.J., 2007. Trace element chemistry of zircons from oceanic crust: A method for distinguishing detrital zircon provenance. Geology 35, 643–646. https://doi.org/10.1130/G23603A.1.
Grosjean, M., Moritz, R., Rezeau, H., Hovakimyan, S., Ulianov, A., Chiaradia, M., Melkonyan, R., 2022. Arabia-Eurasia convergence and collision control on Cenozoic juvenile K-rich magmatism in the South Armenian block. Lesser Caucasus. Earth-Science Rev. 226,. https://doi.org/10.1016/j.earscirev.2022.103949 103949.
Guan, Q., Zhu, D.-C., Zhao, Z.-D., Dong, G.-C., Zhang, L.-L., Li, X.-W., Liu, M., Mo, X.-X., Liu, Y.-S., Yuan, H.-L., 2012. Crustal thickening prior to 38 Ma in southern Tibet: Evidence from lower crust-derived adakitic magmatism in the Gangdese Batholith. Gondwana Res. 21, 88–99. https://doi.org/10.1016/j.gr.2011.07.004.
Haase, K.M., Devey, C.W., 1996. Geochemistry of lavas from the Ahu and Tupa volcanic fields, Easter Hotspot, southeast Pacific: Implications for intraplate magma genesis near a spreading axis. Earth Planet. Sci. Lett. 137, 129–143. https://doi.org/10.1016/0012-821X(95)00217-Z.
Hairapetian, V., Yazdi, M., 2003. Late Devonian conodonts from Dalmeh section, Northeastern Ardekan, Central Iran. Cour. Forschungsinst. Senckenb. 245, 209–225.
Hart, S.R., 1984. A large-scale isotope anomaly in the Southern Hemisphere mantle. Nature 309, 753.
Hart, S.R., Hauri, E.H., Oschmann, L.A., Whitehead, J.A., 1992. Mantle plumes and entrainment: Isotopic evidence. Science (80-) 256, 517–520. https://doi.org/10.1126/science.256.5056.517.
Hassanzadeh, J., Stockli, D.F., Horton, B.K., Axen, G.J., Stockli, L.D., Grove, M., Schmitt, A.K., Walker, J.D., 2008. U-Pb zircon geochronology of late Neoproterozoic-Early Cambrian granitoids in Iran: Implications for paleogeography, magmatism, and exhumation history of Iranian basement. Tectonophysics 451, 71–96. https://doi.org/10.1016/j.tecto.2007.11.062.
Hässig, M., Rolland, Y., Sosson, M., Galoyan, G., Müller, C., Avagyan, A., Sahakyan, L., 2013a. New structural and petrological data on the Amasia ophiolites (NW Sevan-Akera suture zone, Lesser Caucasus): Insights for a large-scale obduction in Armenia and NE Turkey. Tectonophysics 588, 135–153.
Hässig, M., Rolland, Y., Sosson, M., Galoyan, G., Sahakyan, L., Topuz, G., Çelik, Ö.F., Avagyan, A., Müller, C., 2013b. Linking the NE Anatolian and Lesser Caucasus ophiolites: Evidence for large-scale obduction of oceanic crust and implications for the formation of the Lesser Caucasus-Pontides Arc. Geodin. Acta 26, 311–330. https://doi.org/10.1080/09853111.2013.877236.
Hässig, M., Rolland, Y., Sahakyan, L., Sosson, M., Galoyan, G., Avagyan, A., Bosch, D., Müller, C., 2015. Multi-stage metamorphism in the South Armenian Block during the Late Jurassic to Early Cretaceous: Tectonics over south-dipping subduction of Northern branch of Neotethys. J. Asian Earth Sci. 102, 4–23. https://doi.org/10.1016/j.jseaes.2014.07.018.
Hässig, M., Duretz, T., Rolland, Y., Sosson, M., 2016a. Obduction of old oceanic lithosphere due to reheating and plate reorganization: Insights from numerical modelling and the NE Anatolia – Lesser Caucasus case example. J. Geodyn. 96, 35–49. https://doi.org/10.1016/j.jog.2016.02.007.
Hässig, M., Rolland, Y., Duretz, T., Sosson, M., 2016b. Obduction triggered by regional heating during plate reorganization. Terra Nov. 28, 76–82. https://doi.org/10.1111/ter.12193.
Hässig, M., Rolland, Y., Sosson, M., 2017. From seafloor spreading to obduction: Jurassic-Cretaceous evolution of the northern branch of the Neotethys in the Northeastern Anatolian and Lesser Caucasus regions. Geol. Soc. London. Spec. Publ. 428, 41–60.
Hoernle, K., Hauff, F., Kokfelt, T.F., Haase, K., Garbe-Schönberg, D., Werner, R., 2011. On- and off-axis chemical heterogeneities along the South Atlantic Mid-Ocean-Ridge (5–11 S): Shallow or deep recycling of ocean crust and/or intraplate volcanism? Earth Planet. Sci. Lett. 306, 86–97. https://doi.org/10.1016/j.epsl.2011.03.032.
Hou, Z.-Q., Gao, Y.-F., Qu, X.-M., Rui, Z.-Y., Mo, X.-X., 2004. Origin of adakitic intrusives generated during mid-Miocene east–west extension in southern Tibet. Earth Planet. Sci. Lett. 220, 139–155. https://doi.org/10.1016/S0012-821X(04)00007-X.
Jackson, J., McKenzie, D., 1984. Active tectonics of the Alpine-Himalayan Belt between western Turkey and Pakistan. Geophys. J. Int. 77, 185–264. https://doi.org/10.1111/j.1365-246X.1984.tb01931.x.
Jamshidi Badr, M., Collıns, A.S., Masoudı, F., 2013. The U-Pb age, geochemistry and tectonic significance of granitoids in the Soursat Complex, Northwest Iran. Turkish J. Earth Sci. Doi: 10.3906/sag-1301-41.
Jacobsen, S.B., Wasserburg, G.J., 1980. Sm-Nd isotopic evolution of chondrites. Earth Planet. Sci. Lett. 50, 139–155. https://doi.org/10.1016/0012-821X(80)90125-9.
Jochum, K.P., Weis, U., Schwager, B., Stoll, B., Wilson, S.A., Haug, G.H., Andreae, M.O., Enzweiler, J., 2016. Reference values following ISO guidelines for frequently requested rock reference materials. Geostand. Geoanalytical Res. 40, 333–350. https://doi.org/10.1111/j.1751-908X.2015.00392.x.
Jones, D.L., Duncan, R.A., Briden, J.C., Randall, D.E., MacNiocaill, C., 2001. Age of the Batoka basalts, northern Zimbabwe, and the duration of Karoo Large Igneous Province magmatism. Geochemistry, Geophys. Geosystems 2, 2000GC000110. Doi: 10.1029/2000GC000110.
Karsli, O., Dokuz, A., Kandemir, R., 2016. Subduction-related Late Carboniferous to Early Permian Magmatism in the Eastern Pontides, the Camlik and Casurluk plutons: Insights from geochemistry, whole-rock Sr–Nd and in situ zircon Lu–Hf

isotopes, and U-Pb geochronology. Lithos 266–267, 98–114. https://doi.org/10.1016/j.lithos.2016.10.007.
Karyakin, Y.V., 1989. Geodynamics of formation of volcanic complexes of the Lesser Caucasus (in Russian). Proceed. AS USSR. Moscow Nauk. 438, 150.
Kazmin, V.G., 1991. Collision and rifting in the Tethys Ocean: Geodynamic implication. Tectonophysics 196, 371–384. https://doi.org/10.1016/0040-1951(91)90331-L.
Kent, D.V., Irving, E., 2010. Influence of inclination error in sedimentary rocks on the Triassic and Jurassic apparent pole wander path for North America and implications for Cordilleran tectonics. J. Geophys. Res. 115, B10103. https://doi.org/10.1029/2009JB007205.
Khanzatian, H.A., 1992. On the lithological peculiarities of the Darasham–2 section (Nakichevan AR) Upper Permian-Lower Triassic sediments and on the basaltoids sills and stock age (in Russian). Izv. AN. Arm. SSR, Earth Sci. 45, 23–34.
Kharazyan, E.K., 2005. Geological map of Republic of Armenia 1 (500), 000.
Klaver, M., Djuly, T., de Graaf, S., Sakes, A., Wijbrans, J., Davies, G., Vroon, P., 2015. Temporal and spatial variations in provenance of Eastern Mediterranean Sea sediments: Implications for Aegean and Aeolian arc volcanism. Geochim. Cosmochim. Acta 153, 149–168. https://doi.org/10.1016/J.GCA.2015.01.007.
Klaver, M., Matveev, S., Berndt, J., Lissenberg, C.J., Vroon, P.Z., 2017. A mineral and cumulate perspective to magma differentiation at Nisyros volcano. Aegean arc. Contrib. to Mineral. Petrol. 172, 1–23. https://doi.org/10.1007/s00410-017-1414-5.
Knipper, A.L., 1975. The oceanic crust in the Alpine Belt (in Russian). Tr. GIN NAS USSR 267, 207.
Knipper, A.L., Khain, E.V., 1980. Structural position of ophiolites of the Caucasus. Ofioliti. Spec. Issue 2, 297–314.
Koornneef, J.M., Bouman, C., Schwieters, J.B., Davies, G.R., 2013. Use of 10 12 ohm current amplifiers in Sr and Nd isotope analyses by TIMS for application to sub-nanogram samples. J. Anal. At. Spectrom. 28, 749. https://doi.org/10.1039/c3ja30326h.
Kuiper, K.F., Deino, A., Hilgen, F.J., Krijgsman, W., Renne, P.R., Wijbrans, J.R., 2008. Synchronizing rock clocks of Earth history. Science (80-.) 320, 500–504. https://doi.org/10.1126/science.1154339.
Kuscu, I., Gencalioglu Kuscu, G., Tosdal, R.M., Ulrich, T.D., Friedman, R., 2010. Magmatism in the southeastern Anatolian orogenic belt: transition from arc to post-collisional setting in an evolving orogen. Geol. Soc. London. Spec. Publ. 340, 437–460. https://doi.org/10.1144/sp340.19.
Lapierre, H., Bosch, D., Narros, A., Mascle, G.H., Tardy, M., Demant, A., 2007. The Mamonia Complex (SW Cyprus) revisited: Remnant of Late Triassic intra-oceanic volcanism along the Tethyan southwestern passive margin. Geol. Mag. 144, 1–19. https://doi.org/10.1017/S0016756806002937.
Lapierre, H., Samper, A., Bosch, D., Maury, R.C., Béchennec, F., Cotten, J., Demant, A., Brunet, P., Keller, F., Marcoux, J., 2004. The Tethyan plume: Geochemical diversity of Middle Permian basalts from the Oman rifted margin. Lithos 74, 167–198. https://doi.org/10.1016/j.lithos.2004.02.006.
Le Bas, M.J., Le Maitre, R.W., Streckeisen, A., Zanettin, B., 1986. A chemical classification of volcanic rocks based on the total alkali-silica diagram. J. Petrol. 27, 745–750. https://doi.org/10.1093/petrology/27.3.745.
Le Roex, A.P., Dick, H.J.B., Erlank, A.J., Reid, A.M., Frey, F.A., Hart, S.R., 1983. Geochemistry, mineralogy and petrogenesis of lavas erupted along the Southwest Indian Ridge between the Bouvet triple junction and 11 degrees east. J. Petrol. 24, 267–318. https://doi.org/10.1093/petrology/24.3.267.
Le Roex, A.P., Dick, H.J.B., Reid, A.M., Frey, F.A., Erlank, A.J., Hart, S.R., 1985. Petrology and geochemistry of basalts from the American-Antarctic Ridge, Southern Ocean: Implications for the westward influence of the Bouvet mantle plume. Contrib. to Mineral. Petrol. 90, 367–380. https://doi.org/10.1007/BF00384715.
Lee, J.-Y., Marti, K., Severinghaus, J.P., Kawamura, K., Yoo, H.-S., Lee, J.B., Kim, J.S., 2006. A redetermination of the isotopic abundances of atmospheric Ar. Geochim. Cosmochim. Acta 70, 4507–4512. https://doi.org/10.1016/j.gca.2006.06.1563.
Lordkipanidze, M.B., 1980. Alpine volcanism and geodynamics of the central segment of the Mediterranean fold belt. Metsniereba, Tbilisi, p. 162.
Magakyan, R., Sobolev, A.V., Zakariadze, G.S., Kononkova, N.N., 1993. Petrology of evolved boninite magmas: Evidence from the Mesozoic Lesser Caucasus island arc. Petrology 1, 378–394.
Mahmudy Gharaie, M.H., 2002. Sedimentology and geochemistry of the Upper Devonian in Central Iran with special reference to environmental changes leading Frasnian/Famennian boundary event. University of Tokyo.
Mahmudy Gharaie, M.H., Matsumoto, R., Kakuwa, Y., Milroy, P.G., 2004. Late Devonian facies variety in Iran: Volcanism as a possible trigger of the environmental perturbation near the Frasnian-Famennian boundary. Geol. Q. 48, 323–332.
Mart, Y., 1987. Superpositional tectonic patterns along the continental margin of the southeastern Mediterranean: A review. Tectonophysics 140, 213–232. https://doi.org/10.1016/0040-1951(87)90230-7.
Mason, P.R.D., Nikogosian, I.K., van Bergen, M.J., 2008. Major and trace element analysis of melt inclusions by laser ablation ICP-MS. Laser Ablation ICP-MS in the Earth Sciences: Current Practices and Outstanding Issues: Mineralogical Association of Canada Short Course Series 40, 219–240.
McDonough, W.F., Sun, S., -s.,, 1995. The composition of the Earth. Chem. Geol. 120, 223–253. https://doi.org/10.1016/0009-2541(94)00140-4.
McKenzie, D., Bickle, M.J., 1988. The volume and composition of melt generated by extension of the lithosphere. J. Petrol. 29, 625–679. https://doi.org/10.1093/petrology/29.3.625.
McQuarrie, N., van Hinsbergen, D.J.J., 2013. Retrodeforming the Arabia-Eurasia collision zone: Age of collision versus magnitude of continental subduction. Geology 41, 315–318. https://doi.org/10.1130/G33591.1.
Mederer, J., Moritz, R., Zohrabyan, S., Vardanyan, A., Melkonyan, R., Ulianov, A., 2014. Base and precious metal mineralization in Middle Jurassic rocks of the Lesser Caucasus: A review of geology and metallogeny and new data from the Kapan, Alaverdi and Mehmana districts. Ore Geol. Rev. 58, 185–207. https://doi.org/10.1016/J.OREGEOREV.2013.10.007.
Meijers, M.J.M., Smith, B., Kirscher, U., Mensink, M., Sosson, M., Rolland, Y., Grigoryan, A., Sahakyan, L., Avagyan, A., Langereis, C., Müller, C., 2015. A paleolatitude reconstruction of the South Armenian Block (Lesser Caucasus) for the Late Cretaceous: Constraints on the Tethyan realm. Tectonophysics 644, 197–219. https://doi.org/10.1016/j.tecto.2015.01.012.
Meliksetian, B.M., 1989. Petrology, geochemistry and ore genesis of Palaeogene-Neogene volcano-intrusive formations of Lesser Caucasus (magmatism of collision zones). Academy of Science, Tbilisi, Georgian SSR. in Russian.
Menant, A., Jolivet, L., Vrielynck, B., 2016. Kinematic reconstructions and magmatic evolution illuminating crustal and mantle dynamics of the eastern Mediterranean region since the late Cretaceous. Tectonophysics 675, 103–140. https://doi.org/10.1016/j.tecto.2016.03.007.
Milanovsky, E.E., 1968. Neotectonics of the Caucasus. Nedra, Moscow, p. 484. in Russian.
Miyashiro, A., 1978. Nature of alkalic volcanic rock series. Contrib. to Mineral. Petrol. 66, 91–104. https://doi.org/10.1007/BF00376089.
Mohajjel, M., Fergusson, C.L., 2000. Dextral transpression in Late Cretaceous continental collision, Sanandaj-Sirjan Zone, western Iran. J. Struct. Geol. 22, 1125–1139. https://doi.org/10.1016/S0191-8141(00)00023-7.
Moix, P., Beccaletto, L., Kozur, H.W., Hochard, C., Rosselet, F., Stampfli, G.M., 2008. A new classification of the Turkish terranes and sutures and its implication for the paleotectonic history of the region. Tectonophysics 451, 7–39. https://doi.org/10.1016/j.tecto.2007.11.044.
Monster, M., 2016. Multi-method palaeointensity data of the geomagnetic field during the past 500 kyrs from European volcanoes. Utrecht University.
Mouthereau, F., Lacombe, O., Vergés, J., 2012. Building the Zagros collisional orogen: Timing, strain distribution and the dynamics of Arabia/Eurasia plate convergence. Tectonophysics 532–535, 27–60. https://doi.org/10.1016/j.tecto.2012.01.022.
Nikogosian, I.K., Bracco Gartner, A.J.J., van Bergen, M.J., Mason, P.R.D., van Hinsbergen, D.J.J., 2018. Mantle sources of recent Anatolian intraplate magmatism: A regional plume or local tectonic origin? Tectonics 37, 4535–4566. https://doi.org/10.1029/2018TC005219.
Okay, A.I., Sunal, G., Tüysüz, O., Sherlock, S., Keskin, M., Kylander-Clark, A.R.C., 2014. Low-pressure–high-temperature metamorphism during extension in a Jurassic magmatic arc, Central Pontides. Turkey. J. Metamorph. Geol. 32, 49–69. https://doi.org/10.1111/jmg.12058.
Okay, A.I., Tüysüz, O., 1999. Tethyan sutures of northern Turkey. Geol. Soc. London. Spec. Publ. 156, 475–515. https://doi.org/10.1144/GSL.SP.1999.156.01.22.
Okay, A.I., Zattin, M., Cavazza, W., 2010. Apatite fission-track data for the Miocene Arabia-Eurasia collision. Geology 38, 35–38. https://doi.org/10.1130/G30234.1.
Osozawa, S., Usuki, T., Usuki, M., Wakabayashi, J., Jahn, B.-M., 2019. Trace elemental and Sr-Nd-Hf isotopic compositions, and U-Pb ages for the Kitakami adakitic plutons: Insights into interactions with the early Cretaceous TRT triple junction offshore Japan. J. Asian Earth Sci. 184,. https://doi.org/10.1016/j.jseaes.2019.103968 103968.
Othman, D.B., White, W.M., Patchett, J., 1989. The geochemistry of marine sediments, island arc magma genesis, and crust-mantle recycling. Earth Planet. Sci. Lett. 94, 1–21. https://doi.org/10.1016/0012-821X(89)90079-4.
Özgül, N., 1984. Stratigraphy and tectonic evolution of the Central Taurides, in: Tekeli, O., Göncüoğlu, M.C. (Eds.), Geology of the Taurus Belt. Proceedings of the International Tauride Symposium. MTA Ankara, Cambridge, UK, pp. 77–90.
Paffenholz, K.N., 1952. Geological map of Armenian SSR and adjacent parts of Lesser Caucasus 1 (200), 000.
Pearce, J.A., 1982. Trace element characteristics of lavas from destructive plate boundaries. In: Thorpe, R.S. (Ed.), Andesites: Orogenic Andesites and Related Rocks. John Wiley & Sons, New York, NY, pp. 525–548.
Pearce, J.A., Harris, N.B., Tindle, A.G., 1984. Trace element discrimination diagrams for the tectonic interpretation of granitic rocks. J. Petrol. 25, 956–983. https://doi.org/10.1093/petrology/25.4.956.
Peccerillo, A., Taylor, S.R., 1976. Geochemistry of Eocene calc-alkaline volcanic rocks from the Kastamonu area. Northern Turkey. Contrib. to Mineral. Petrol. 58, 63–81. https://doi.org/10.1007/BF00384745.
Ramezani, J., Tucker, R.D., 2003. The Saghand region, Central Iran: U-Pb geochronology, petrogenesis and implications for Gondwana tectonics. Am. J. Sci. 303, 622–665. https://doi.org/10.2475/ajs.303.7.622.
Robertson, A.H.F., Ustaömer, T., Pickett, E.A., Collins, A.S., Andrew, T., Dixon, J.E., 2004. Testing models of Late Palaeozoic-Early Mesozoic orogeny in Western Turkey: Support for an evolving open-Tethys model. J. Geol. Soc. London. 161, 501–511. https://doi.org/10.1144/0016-764903-080.
Rolland, Y., 2017. Caucasus collisional history: Review of data from East Anatolia to West Iran. Gondwana Res. 49, 130–146. https://doi.org/10.1016/j.gr.2017.05.005.

Rolland, Y., Galoyan, G., Bosch, D., Sosson, M., Corsini, M., Fornari, M., Verati, C., 2009. Jurassic back-arc and Cretaceous hot-spot series in the Armenian ophiolites – Implications for the obduction process. Lithos 112, 163–187. https://doi.org/10.1016/j.lithos.2009.02.006.

Rolland, Y., Galoyan, G., Sosson, M., Melkonyan, R., Avagyan, A., 2010. The Armenian Ophiolite: insights for Jurassic back-arc formation, Lower Cretaceous hot spot magmatism and Upper Cretaceous obduction over the South Armenian Block. Geol. Soc. London. Spec. Publ. 340, 353–382. https://doi.org/10.1144/SP340.15.

Rolland, Y., Perincek, D., Kaymakci, N., Sosson, M., Barrier, E., Avagyan, A., 2012. Evidence for 80–75 Ma subduction jump during Anatolide–Tauride–Armenian block accretion and 48 Ma Arabia-Eurasia collision in Lesser Caucasus-East Anatolia. J. Geodyn. 56–57, 76–85. https://doi.org/10.1016/J.JOG.2011.08.006.

Rolland, Y., Hässig, M., Bosch, D., Bruguier, O., Melis, R., Galoyan, G., Topuz, G., Sahakyan, L., Avagyan, A., Sosson, M., 2020. The East Anatolia-Lesser Caucasus ophiolite: An exceptional case of large-scale obduction, synthesis of data and numerical modelling. Geosci. Front. 11, 83–108. https://doi.org/10.1016/j.gsf.2018.12.009.

Saccani, E., Azimzadeh, Z., Dilek, Y., Jahangiri, A., 2013b. Geochronology and petrology of the Early Carboniferous Misho Mafic Complex (NW Iran), and implications for the melt evolution of Paleo-Tethyan rifting in Western Cimmeria. Lithos 162–163, 264–278. https://doi.org/10.1016/j.lithos.2013.01.008.

Saccani, E., Allahyari, K., Rahimzadeh, B., 2014. Petrology and geochemistry of mafic magmatic rocks from the Sarve-Abad ophiolites (Kurdistan region, Iran): Evidence for interaction between MORB-type asthenosphere and OIB-type components in the southern Neo-Tethys Ocean. Tectonophysics 621, 132–147. https://doi.org/10.1016/j.tecto.2014.02.011.

Saccani, E., Photiades, A., 2005. Petrogenesis and tectonomagmatic significance of volcanic and subvolcanic rocks in the Albanide-Hellenide ophiolitic melanges. Isl. Arc 14, 494–516. https://doi.org/10.1111/j.1440-1738.2005.00480.x.

Saccani, E., Delavari, M., Beccaluva, L., Amini, S., 2010. Petrological and geochemical constraints on the origin of the Nehbandan ophiolitic complex (eastern Iran): Implication for the evolution of the Sistan Ocean. Lithos 117, 209–228. https://doi.org/10.1016/j.lithos.2010.02.016.

Saccani, E., Allahyari, K., Beccaluva, L., Bianchini, G., 2013a. Geochemistry and petrology of the Kermanshah ophiolites (Iran): Implication for the interaction between passive rifting, oceanic accretion, and OIB-type components in the Southern Neo-Tethys Ocean. Gondwana Res. 24, 392–411. https://doi.org/10.1016/j.gr.2012.10.009.

Schandl, E.S., Gorton, M.P., 2002. Application of high field strength elements to discriminate tectonic settings in VMS environments. Econ. Geol. 97, 629–642. https://doi.org/10.2113/gsecongeo.97.3.629.

Schilling, J.G., Zajac, M., Evans, R., Johnston, T., White, W., Devine, J.D., Kingsley, R., 1983. Petrologic and geochemical variations along the Mid-Atlantic Ridge from 29 degrees N to 73 degrees N. Am. J. Sci. 283, 510–586. https://doi.org/10.2475/ajs.283.6.510.

Şengör, A.M.C., 1987. Tectonics of the Tethysides: Orogenic collage development in a collisional setting. Annu. Rev. Earth Planet. Sci. 15, 213–244.

Şengör, A.M.C., 1990. A new model for the late Palaeozoic—Mesozoic tectonic evolution of Iran and implications for Oman. Geol. Soc. London. Spec. Publ. 49, 797–831. https://doi.org/10.1144/GSL.SP.1992.049.01.49.

Şengör, A.M.C., Lom, N., Sunal, G., Zabcı, C., Sancar, T., 2019a. The phanerozoic palaeotectonics of Turkey. Part I: An inventory. Mediterr. Geosci. Rev. 1, 91–161. https://doi.org/10.1007/s42990-019-00007-3.

Şengör, A.M.C., Lom, N., Zabcı, C., Sunal, G., Sançar, T., 2019b. On the nature of the Cimmerian Continent and the opening of the Neo-Tethys. Geophys. Res. Abstr.

Şengör, A.M.C., Yilmaz, Y., 1981. Tethyan evolution of Turkey: A plate tectonic approach. Tectonophysics 75, 181–241. https://doi.org/10.1016/0040-1951(81)90275-4.

Serobyan, V., Grigoryan, A., Mottequin, B., Mayilyan, R., Crônier, C., Danelian, T., 2019. Biostratigraphy of the Upper Devonian trigonirhynchiid brachiopods (rhynchonellida) from Armenia. Proc. NAS RA, Earth Sci. 72, 3–18.

Shafaii Moghadam, H., Khademi, M., Hu, Z., Stern, R.J., Santos, J.F., Wu, Y., 2015. Cadomian (Ediacaran-Cambrian) arc magmatism in the ChahJam-Biarjmand metamorphic complex (Iran): Magmatism along the northern active margin of Gondwana. Gondwana Res. 27, 439–452. https://doi.org/10.1016/j.gr.2013.10.014.

Shafaii Moghadam, H., Stern, R.J., 2014. Ophiolites of Iran: Keys to understanding the tectonic evolution of SW Asia: (I) Paleozoic ophiolites. J. Asian Earth Sci. 91, 19–38. https://doi.org/10.1016/J.JSEAES.2014.04.008.

Shafaii Moghadam, H., Stern, R.J., 2015. Ophiolites of Iran: Keys to understanding the tectonic evolution of SW Asia: (II) Mesozoic ophiolites. J. Asian Earth Sci. 100, 31–59. https://doi.org/10.1016/j.jseaes.2014.12.016.

Shakerardakani, F., Neubauer, F., Liu, X., Bernroider, M., Monfaredi, B., von Quadt, A., 2018. Tectonic significance of Triassic mafic rocks in the June Complex, Sanandaj-Sirjan zone. Iran. Swiss J. Geosci. 111, 13–33. https://doi.org/10.1007/s00015-017-0281-4.

Sheikholeslami, M.R., Pique, A., Mobayen, P., Sabzehei, M., Bellon, H., Emami, M.H., 2008. Tectono-metamorphic evolution of the Neyriz metamorphic complex, Quri-Kor-e-Sefid area (Sanandaj-Sirjan Zone, SW Iran). J. Asian Earth Sci. 31, 504–521. https://doi.org/10.1016/j.jseaes.2007.07.004.

Shellnutt, J.G., Bhat, G.M., Wang, K.L., Brookfield, M.E., Jahn, B.M., Dostal, J., 2014. Petrogenesis of the flood basalts from the Early Permian Panjal Traps, Kashmir, India: Geochemical evidence for shallow melting of the mantle. Lithos 204, 159–171. https://doi.org/10.1016/j.lithos.2014.01.008.

Sokół, K., Halama, R., Meliksetian, K., Savov, I.P., Navasardyan, G., Sudo, M., 2018. Alkaline magmas in zones of continental convergence: The Tezhsar volcano-intrusive ring complex, Armenia. Lithos 320–321, 172–191. https://doi.org/10.1016/j.lithos.2018.08.028.

Sosson, M., Rolland, Y., Müller, C., Danelian, T., Melkonyan, R., Kekelia, S., Adamia, S., Babazadeh, V., Kangarli, T., Avagyan, A., 2010. Subductions, obduction and collision in the Lesser Caucasus (Armenia, Azerbaijan, Georgia), new insights. Geol. Soc. London. Spec. Publ. 340, 329–352. https://doi.org/10.1144/SP340.14.

Stampfli, G.M., 2000. Tethyan oceans. Geol. Soc. London. Spec. Publ. 173, 1–23. https://doi.org/10.1144/GSL.SP.2000.173.01.01.

Stampfli, G.M., Borel, G.D., 2002. A plate tectonic model for the Paleozoic and Mesozoic constrained by dynamic plate boundaries and restored synthetic oceanic isochrons. Earth Planet. Sci. Lett. 196, 17–33. https://doi.org/10.1016/S0012-821X(01)00588-X.

Stampfli, G., Marcoux, J., Baud, A., 1991. Tethyan margins in space and time. Palaeogeogr. Palaeoclimatol. Palaeoecol. 87, 373–409. https://doi.org/10.1016/0031-0182(91)90142-E.

Sun, S.S., McDonough, W.F., 1989. Chemical and isotopic systematics of oceanic basalts: Implications for mantle composition and processes. In: Saunders, A.D., Norry, M.J. (Eds.), Magmatism in the Ocean Basins. Geological Society Special Publication, pp. 313–345. https://doi.org/10.1144/GSL.SP.1989.042.01.19.

Svensen, H.H., Torsvik, T.H., Callegaro, S., Augland, L., Heimdal, T.H., Jerram, D.A., Planke, S., Pereira, E., 2018. Gondwana Large Igneous Provinces: plate reconstructions, volcanic basins and sill volumes. Geol. Soc. London. Spec. Publ. 463, 17–40. https://doi.org/10.1144/SP463.7.

Teipel, U., Eichhorn, R., Loth, G., Rohrmüller, J., Höll, R., Kennedy, A., 2004. U-Pb SHRIMP and Nd isotopic data from the western Bohemian Massif (Bayerischer Wald, Germany): Implications for Upper Vendian and Lower Ordovician magmatism. Int. J. Earth Sci. 93, 782–801. https://doi.org/10.1007/s00531-004-0419-2.

Topuz, G., Celik, O.F., Sengor, A.M.C., Altintas, I.E., Zack, T., Rolland, Y., Barth, M., 2013a. Jurassic ophiolite formation and emplacement as backstop to a subduction-accretion complex in northeast Turkey, the Refahiye ophiolite, and relation to the Balkan ophiolites. Am. J. Sci. 313, 1054–1087. https://doi.org/10.2475/10.2013.04.

Topuz, G., Göçmengil, G., Rolland, Y., Çelik, Ö.F., Zack, T., Schmitt, A.K., 2013b. Jurassic accretionary complex and ophiolite from northeast Turkey: No evidence for the Cimmerian continental ribbon. Geology 41, 255–258. https://doi.org/10.1130/G33577.1.

Topuz, G., Okay, A.I., Altherr, R., Schwarz, W.H., Sunal, G., Altinkaynak, L., 2014. Triassic warm subduction in northeast Turkey: Evidence from the Ağvanis metamorphic rocks. Isl. Arc 23, 181–205. https://doi.org/10.1111/iar.12068.

Topuz, G., Candan, O., Zack, T., Yilmaz, A., 2017. East Anatolian plateau constructed over a continental basement: No evidence for the East Anatolian accretionary complex. Geology 45, 791–794. https://doi.org/10.1130/G39111.1.

Topuz, G., Okay, A.I., Schwarz, W.H., Sunal, G., Altherr, R., Kylander-Clark, A.R.C., 2018. A middle Permian ophiolite fragment in Late Triassic greenschist- to blueschist-facies rocks in NW Turkey: An earlier pulse of suprasubduction-zone ophiolite formation in the Tethyan belt. Lithos 300–301, 121–135. https://doi.org/10.1016/j.lithos.2017.12.005.

Torsvik, T.H., Cocks, L.R.M., 2013. Gondwana from top to base in space and time. Gondwana Res. 24, 999–1030. https://doi.org/10.1016/j.gr.2013.06.012.

Torsvik, T.H., van der Voo, R., Preeden, U., Mac Niocaill, C., Steinberger, B., Doubrovine, P.V., van Hinsbergen, D.J.J., Domeier, M., Gaina, C., Tohver, E., Meert, J.G., McCausland, P.J.A., Cocks, L.R.M., 2012. Phanerozoic polar wander, palaeogeography and dynamics. Earth-Science Rev. 114, 325–368. https://doi.org/10.1016/j.earscirev.2012.06.007.

Ustaömer, T., Robertson, A.H.F., Ustaömer, P.A., Gerdes, A., Peytcheva, I., 2013. Constraints on Variscan and Cimmerian magmatism and metamorphism in the Pontides (Yusufeli–Artvin area), NE Turkey from U-Pb dating and granite geochemistry. Geol. Soc. London. Spec. Publ. 372, 49–74. https://doi.org/10.1144/SP372.13.

Ustaömer, P.A., Ustaömer, T., Robertson, A.H.F., 2012. Ion probe U-Pb dating of the central Sakarya basement: A peri-Gondwana terrane intruded by Late Lower Carboniferous subduction/collision-related granitic rocks. Turkish J. Earth Sci. 21, 905–932. https://doi.org/10.3906/yer-1103-1.

van der Boon, A., van Hinsbergen, D.J.J., Rezaeian, M., Gürer, D., Honarmand, M., Pastor-Galán, D., Krijgsman, W., Langereis, C.G., 2018. Quantifying Arabia-Eurasia convergence accommodated in the Greater Caucasus by paleomagnetic reconstruction. Earth Planet. Sci. Lett. 482, 454–469. https://doi.org/10.1016/j.epsl.2017.11.025.

van Hinsbergen, D.J.J., Maffione, M., Plunder, A., Kaymakcı, N., Ganerød, M., Hendriks, B.W.H., Corfu, F., Gürer, D., de Gelder, G.I.N.O., Peters, K., McPhee, P.J., Brouwer, F.M., Advokaat, E.L., Vissers, R.L.M., 2016. Tectonic evolution and paleogeography of the Kırşehir Block and the Central Anatolian Ophiolites, Turkey. Tectonics 35, 983–1014. https://doi.org/10.1002/2015TC004018.

van Hinsbergen, D.J.J., Torsvik, T.H., Schmid, S.M., Maţenco, L.C., Maffione, M., Vissers, R.L.M., Gürer, D., Spakman, W., 2020. Orogenic architecture of the Mediterranean region and kinematic reconstruction of its tectonic evolution since the Triassic. Gondwana Res. 81, 79–229. https://doi.org/10.1016/j.gr.2019.07.009.

Wang, M., Li, C., Zeng, X.-W., Li, H., Fan, J.-J., Xie, C.-M., Hao, Y.-J., 2019. Petrogenesis of the southern Qiangtang mafic dykes, Tibet: Link to a late Paleozoic mantle plume on the northern margin of Gondwana? Geol. Soc. Am. Bull. https://doi.org/10.1130/B35110.1.

Wendt, J., Kaufmann, B., Belka, Z., Farsan, N., Bavandpur, A.K., 2002. Devonian/Lower Carboniferous stratigraphy, facies patterns and palaeogeography of Iran. Part I. Southeastern Iran. Acta Geol. Pol. 52, 129–168.

Wiedenbeck, M., Hanchar, J.M., Peck, W.H., Sylvester, P., Valley, J., Whitehouse, M., Kronz, A., Morishita, Y., Nasdala, L., Fiebig, J., Franchi, I., Girard, J.-P., Greenwood, R.C., Hinton, R., Kita, N., Mason, P.R.D., Norman, M., Ogasawara, M., Piccoli, P.M., Rhede, D., Satoh, H., Schulz-Dobrick, B., Skår, O., Spicuzza, M.J., Terada, K., Tindle, A., Togashi, S., Vennemann, T., Xie, Q., Zheng, Y.-F., 2004. Further characterisation of the 91500 zircon crystal. Geostand. Geoanalytical Res. 28, 9–39. https://doi.org/10.1111/j.1751-908X.2004.tb01041.x.

Wijbrans, J.R., Pringle, M.S., Koppers, A.A.P., Scheveers, R., 1995. Argon geochronology of small samples using the Vulkaan argon laserprobe. Proc. R. Netherlands Acad. Arts Sci. 98, 185–218.

Willbold, M., Stracke, A., 2006. Trace element composition of mantle end-members: Implications for recycling of oceanic and upper and lower continental crust. Geochemistry. Geophys. Geosystems 7, 1–30. https://doi.org/10.1029/2005GC001005.

Xu, W., Dong, Y., Zhang, X., Deng, M., Zhang, L., 2016. Petrogenesis of high-Ti mafic dykes from Southern Qiangtang, Tibet: Implications for a ca. 290 Ma large igneous province related to the early Permian rifting of Gondwana. Gondwana Res. 36, 410–422. https://doi.org/10.1016/j.gr.2015.07.016.

Yilmaz, A., Adamia, S., Yilmaz, H., 2014. Comparisons of the suture zones along a geotraverse from the Scythian Platform to the Arabian Platform. Geosci. Front. 5, 855–875. https://doi.org/10.1016/j.gsf.2013.10.004.

Yilmaz, A., Yilmaz, H., 2013. Ophiolites and ophiolitic mélanges of Turkey: A review. Geol. Bull, Turkey, p. 56.

Yilmaz, A., Yilmaz, H., Kaya, C., Boztug, D., 2010. The nature of the crustal structure of the Eastern Anatolian Plateau. Turkey. Geodin. Acta 23, 167–183. https://doi.org/10.3166/ga.23.167-183.

Yogodzinski, G.M., Brown, S.T., Kelemen, P.B., Vervoort, J.D., Portnyagin, M., Sims, K.W.W., Hoernle, K., Jicha, B.R., Werner, R., 2015. The role of subducted basalt in the source of island arc magmas: Evidence from seafloor lavas of the western Aleutians. J. Petrol. 56, 441–492. https://doi.org/10.1093/petrology/egv006.

Zanchi, A., Zanchetta, S., Berra, F., Mattei, M., Garzanti, E., Molyneux, S., Nawab, A., Sabouri, J., 2009. The Eo-Cimmerian (Late? Triassic) orogeny in North Iran. Geol. Soc. London. Spec. Publ. 312, 31–55. https://doi.org/10.1144/SP312.3.

Zeng, Y.-C., Xu, J.-F., Ducea, M.N., Chen, J.-L., Huang, F., Zhang, L., 2019. Initial rifting of the Lhasa Terrane from Gondwana: insights from the Permian (~262 Ma) amphibole-rich lithospheric mantle-derived Yawa basanitic intrusions in southern Tibet. J. Geophys. Res. Solid Earth 2018JB016281. https://doi.org/10.1029/2018JB016281.

Zindler, A., Hart, S., 1986. Chemical geodynamics. Annu. Rev. Earth Planet. Sci. 14, 493–571.